Determination of rheological properties of Power-law fluids using a numerical ultrasonic waveguide viscometer

by

Olivier Schuringa

to obtain the degree of Master of Science
at the Delft University of Technology,
to be defended publicly on July 14th, 2021.

Student number:	4367995	
Project duration:	September 1st, 2020 – July 14th, 2021	
Thesis committee:	Dr. ir. M. Rohde,	TU Delft, supervisor
	Prof. dr. ir. J. L. Kloosterman,	TU Delft
	Prof. dr. ir. D. J. Verschuur,	TU Delft

An electronic version of this thesis is available at https://www.martinrohde.nl/.

TU Delft Delft University of Technology

Abstract

The Molten Salt Fast Reactor (MSFR) is one of the new Generation-IV type reactors which are according to the Energy Road Map 2050 of the European Union important contributors to the decarbonisation of the energy supply. The SAMOSAFER (Severe Accident MOdeling and Safety Assessment for Fluid-fuel Energy Reactors) project aims to develop and demonstrate new safety barriers for molten salt reactors based on new simulation models and tools validated with experiments. In order to predict and study the behaviour of this fuel salt in the MSFR properties such as the density and rheology have to be known to predict the flow and neutronic behaviour of the fuel. Due to practical limitations inflicted by the molten salt, its high temperature and radioactivity, to determine the rheology of the fuel an ultrasonic instrument using a shear-wave and waveguide is used to overcome these limitations. Since the molten salt is suspected to be a non-Newtonian fluid, the fluid type that will be investigated is the Power-law fluid type. This research will focus on the development of measurement methods to retrieve the rheological properties, the flow index m and the consistency index K_m, of Power-law fluids with amplitude measurements of the ultrasonic shear-wave viscometer using a numerical model. To develop such methods the analytical expression of the shear-rate in a Power-law fluid is necessary, but unknown. In this research three analytical expression of the shear-rate in a Power-law fluid are proposed and six methods developed. The fluids used in this research are ketchup (shear-thinning), soybean oil (shear-thinning) and ethylene-glycol (shear-thickening).

The methods I, II, III and IV are used to find the rheological properties m and K_m with an expression of the shear-rate based on the result of Ai & Vafai [13], first proposed by Rohde [11]. The shear-rate used in methods I, II, III, IV turned out to be incorrect, but the expression used to determine the flow index m in method IV remains valid and experimentally usable. Method V uses a different expression of the shear-rate in a Power-law fluid compared to methods I, II, III and IV. The results of this method for the flow index m are unchanged compared to results of method IV and the values for the consistency indices K_m deviated from the literature values of the used fluids. Method VI uses an alternative expression of the shear-rate in a Power-law fluid compared to methods I, II, III, IV and V. Within method VI two approaches are used to determine the rheological properties m, K_m, namely: Approach A and Approach B. Approach A can only be used numerically, but Approach B can be used experimentally. Both Approach A and Approach B of method VI gave accurate results for the flow index m and the results of the consistency indices K_m have the same order of magnitude as the literature values of the used fluids.

In future studies the shear-rate on the boundary of Power-law fluids needs to be studied more extensively to obtain more accurate results for the consistency indices. Also, the numerical viscometer needs to be extended for other types of fluids such as Bingham and Casson fluids. This will eventually contribute to the final goal of SAMOSAFER to ensure that the MSFR can comply with all expected regulations in 30 years' time.

Contents

Chapter 1

Introduction

The increasing clean energy demand is one of the most important issues of the world of today. Oil, gas and coal are a cheap and immediate energy source, but they will eventually finish and can have a negative effect on the climate of this planet. Solar and wind energy are good alternatives for reducing the carbon emission but cannot produce the same amount of energy as the before-mentioned fossil fuels. Although nuclear energy can yield an enormous amount of energy, is sustainable and reliable, controversial arguments exist because of the safety concerns and historic accidents, for instance Chernobyl (1986) and Fukushima (2011). These crises have changed the look on nuclear power generation and its advantages and disadvantages.

In the year 2000, during the Generation IV International Forum, six new types of nuclear reactors were proposed [1] to deal with the significant safety concerns. These new generation of reactors were designed to excel in the area of safety. The Molten Salt Fast Reactor (MSFR) is one of this new generation reactors. According to the Energy Road Map 2050 of the European Union nuclear energy is an important contributor to the decarbonisation of the energy supply [2]. In order to stimulate the feasibility of implementation of these new type of reactors the SAMOSAFER project as part of the Horizon 2020 program was initiated. SAMOSAFER (Severe Accident MOdeling and Safety Assessment for Fluid-fuel Energy Reactors) aims to develop and demonstrate new safety barriers for more controlled behaviour of molten salt reactors in severe accidents, based on new simulation models and tools validated with experiments. The grand objective is to ensure that the molten salt reactor can comply with all expected regulations in 30 years time [3]. This research is part of the SAMOSAFER project.

1.1 The Molten Salt Fast Reactor

Most nuclear reactor which are in operation today use solid fuel, such as uranium rods, in a water-filled vessel, sometimes pressurised. The Molten Salt Fast Reactor (MSFR) uses a liquid fuel salt in a cylindrical vessel under ambient pressure at an operating temperature of 750 °C [4]. This new type of nuclear reactor design allows the flexibility of adapting the fuel salt composition during reactor operation. Also, the MSFR is intrinsically safer than the nuclear reactors which are currently operated around the world. In case of loss of power, it

uses a freeze plug system in order to drain the liquid fuel salt in safe tanks under the reactor. Other advantages are that the fuel salt serves both the function of being the heat transfer medium and the coolant and since the liquid expands when heated there is negative feedback on the rate of nuclear reaction [4].

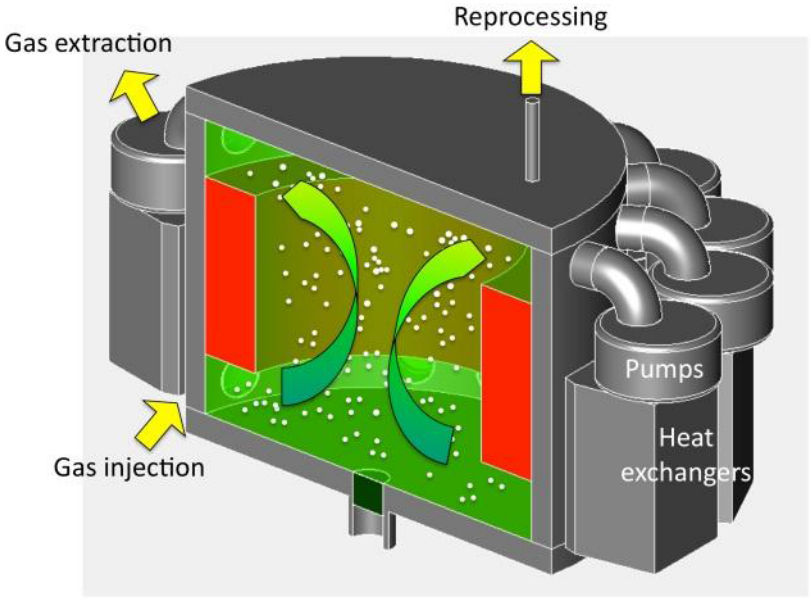

Figure 1.1: Schematic layout of MSFR [3]

For the MSFR to reach SAMOSAFER's goal still a significant amount of research is needed. One part of this research investigates the molten salt itself. Part of the research being done at the Reactor Institute Delft (RID) is about the fundamental behaviour and properties of the used fuel salt. It uses a fluoride salt with the composition of LiF-ThF_4-UF_4-PuF_3 [5]. In order to predict and study the behaviour of this fuel salt in the MSFR certain properties have to be known, such as the density and rheology. This research will focus mainly on the development of a measurement method of the rheology using ultrasonic waves.

1.2 The ultrasonic viscometer

A wide range of viscometers exists to determine the viscosity of various different types of fluids. However, due to the particular nature of the molten fuel salt there are some practical limitations that need to be overcome. The most significant of these limitations are the high temperature of 750 °C, its radioactivity and highly corrosive nature. Also, previous research estimated that the viscosity of this fuel salt will be between 3-13 [mPa·s] [6] which requires a sensitive measuring technique. In order to overcome these limitation a measurement setup is proposed using ultrasonic shear-waves through a waveguide partially immersed in the fluid of interest for the determination of the rheology.

The method of using ultrasonic waves for the determination of viscosity was originally proposed by Mason [7] which used an ultrasonic pulse send directly through the fluid by a transducer in contact with the fluid. The idea behind this method is that the returned signal has lost a certain amount of energy, attenuation of the wave energy, which can be related to properties of the fluid such as the viscosity.

In research done by Vogt [8] techniques using a waveguide were developed and investigated. Waveguides can have a multitude of shapes and be made of different materials which can have an impact on the properties of the wave that needs to be guided. It should be noted however that the waveguide also has a second function of separating the transducer from the fluid itself since its very high temperature would increase the transducer's temperature above the Curie temperature, which causes the loss of piezoelectric activity [9].

Research done by Cegla [10] investigated fluid characterisation and non-destructive testing in harsh environments using guided ultrasonic waves. It showed that a variety of guided compressional, flexural and shear horizontal wave modes can exist in a steel plate as waveguide depending on the product between the thickness of the plate and the frequency of the wave mode. This makes that one can tweak their waveguide and frequency to their advantage. Therefore, in this research the waveguide selected will be a very thin rectangular plate in combination with a transducer producing a shear-wave, see figure 1.2.

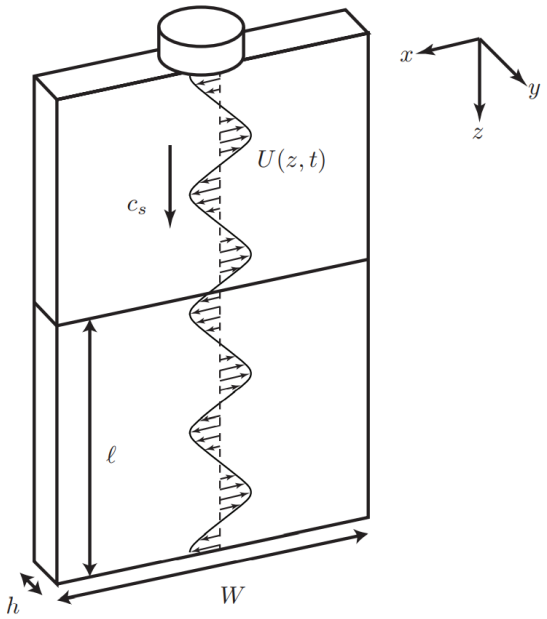

Figure 1.2: Schematic setup of the ultrasonic shear-wave viscometer [11]. The transducer at the top produces a shear-wave travelling in the z-direction and polarised in the x-direction with $U(z,t)$ the amplitude at time t and position z in a partially immersed waveguide, where l is the immersion depth, c_s the shear-wave speed, h and W are the waveguide's thickness and width respectively.

The advantages of a shear-wave in combination with a very thin plate as waveguide is that there is no energy loss at the end of the waveguide and it is a non-dispersive wave, resulting in an attenuated signal solely due to viscous effect. The benefit of using a non-dispersive wave is that the shape of the wave will be conserved over the propagation path.

1.3 Rheology of a fluid

In the proposed viscometer setup the attenuation of the signal can be linked to the viscosity of the fluid. One can imagine that the more viscous a fluid, the larger the resulting attenuation of the signal. However, one can also imagine that the viscosity of a fluid may not always have a constant value. The velocity gradient in the fluid due to a shear-wave, also known as the shear-rate, plays a major role in this viscous behaviour. The study that deals with how materials flow as a function of the shear-rate is called rheology. It roughly divides fluids in two distinct groups: fluids which viscosities are independent of the shear-rate, *Newtonian fluids*, and fluids which viscosities dependent on the shear-rate, *Non-Newtonian fluids*. There are several different types non-Newtonian fluids such as but not limited to Power-law, Bingham and Casson fluids which all respond differently to the shear-rate.

In this research the fluid type that will be investigated is the Power-law fluid since the molten salt in MSFR is suspected to be a non-Newtonian fluid. The focus of this research will therefore be to develop experimental methods to retrieve the rheological properties of known Power-law fluids. To find these properties an expression of the shear-stress in a Power-law fluid is needed. This shear-stress as a function of the shear-rate is given by the following equation (*the Ostwald-de Waele relationship*):

$$\tau_{PL}(\dot{\gamma}) = -\mu_{app}(\dot{\gamma}) \cdot \dot{\gamma} \tag{1.1}$$

$$\mu_{app}(\dot{\gamma}) = K_m \cdot |\dot{\gamma}|^{m-1} \tag{1.2}$$

where $\dot{\gamma}$ [s^{-1}] is the shear-rate or velocity gradient perpendicular to the shear plane, K_m [Pa·s^m] is called the consistency index and m [-] the flow index. These two constants together are called the rheological properties and they characterise the type of Power-law fluid. Note that viscosity in this type of fluids is called the apparent viscosity.

1.4 Previous research

This proposed ultrasonic waveguide viscometer has been investigated experimentally by Rook [12] in case of a Newtonian fluid. Rook showed that at room temperature good viscosity measurements for low viscosity Newtonian fluids can be obtained. One of the reasons this method is possible is because there exists an analytical solution to the velocity profile for a Newtonian fluid to find the shear-rate. By using this expression a solution can be provided to find the viscosity of this fluid. In case of non-Newtonian fluids such as Power-law fluids there does not exist such an analytical expression and therefore the rheological properties for a Power-law fluid cannot be determined in the same way as in the case of Rook.

In order to find the rheological properties of a Power-law fluid, Rohde [11] proposed a solution to the shear-rate based on the results of Ai & Vafai [13]. Making using of a numerical model to mimic the ultrasonic viscometer setup, Borstlap [14] investigated this proposed solution to find the rheological properties m and K_m. One of the conclusions of this research is that the used solution of Rohde was suitable for determination of the flow index m, but measurements on the consistency index K_m asks for a more accurate method.

1.5 Research goals and thesis outline

The ultimate goal of this research would be that there can be concluded that the rheology of any fluid can be determined by using this ultrasonic waveguide viscometer. In order to reach this goal questions need answering. One of the more general research questions is the following:

* How can the rheological properties of power-law fluids be accurately retrieved from the amplitude measurements of the ultrasonic shear-wave waveguide viscometer?

This question is taken as a starting point of this research since it is not fully answered by previous research. It was found by Borstlap that the flow index m could be retrieved accurately by using a linear fitting method, but the determination of the consistency index K_m was inaccurate since K_m had a high sensitivity for small variations of m. In this research the obtained amplitude measurements for different immersion depths, is fitted to a linear function, but it is possible that other functions are more desirable for the measurement of K_m and m. Although it is interesting to find out where this sensitivity comes from another question also comes to mind:

* Is the linear fitting method proposed by Rohde ideal for the determination of the flow and consistency index?

This method also relies on measuring the attenuated amplitude signal with the immersion depth as only parameter, but the frequency of the signal can also be used. Therefore:

* Can the rheological properties m and K_m be determined by using the immersion depth of the waveguide in the fluid and the frequency as variables?

Now, if the rheological properties of known power-law fluids can be determined numerically accurately, it would be an insightful addition to the research if for the same power-law fluids these properties would be determined with an actual measuring setup in order to compare results.

This master's thesis is divided in multiple chapters to retain clarity. In chapter 2 the necessary theory will be discussed after which chapter 3 is used to set out the used methods. This research will make use of a numerical simulation model made in Python, rather than make use of large simulation programs such as COMSOL Multiphysics. In chapter 4 the results of this research are shown and in chapter 5 conclusions are drawn and recommendations are made.

Chapter 2

Theory

In this chapter the theoretical background of the ultrasonic waveguide viscometer is covered and the difference between immersion in a Newtonian fluid and a Power-law fluid will be discussed. The goal of this chapter is to make clear how the solution to the energy equation of the ultrasonic wave in the waveguide immersed in a Power-law fluid can be obtained since this expression is needed to investigate the rheology. In order to do this, the expression of the shear-rate on the boundary in a Power-law fluid needs to be known and because this expression is not known analytically, three different expressions for the shear-rate on the boundary in a Power-law fluid are proposed in this chapter.

2.1 The wave and waveguide

In this research two different waves are discussed, namely (I) the wave in the waveguide created by the transducer and (II) the wave in the fluid created by wave in the waveguide due to friction. Wave (I) is depicted in figure 1.2 in the partially immersed waveguide and it loses its energy by the creation of a secondary wave (II), described in section 2.2. Obviously, the shape of the waveguide and the type of wave created by the transducer have an influence on energy loss of wave (I) when partially immersed. Therefore, the question is: what type of wave and what shape of the waveguide should be used?

In this research there is made use of *shear ultrasonic waves* in combination with a *thin rectangular steel plate as waveguide*. These shear-waves travel in z-direction and are polarised in the x-direction, see figure 1.2. According to a result obtained by Cegla [10] which can be seen in figure 2.1, for a certain range of the *frequency thickness product*, namely between 0 - 1.5 [MHz·mm], the only shear-wave mode that can exist is the fundamental shear-wave (SH0). Also, the phase velocity of this fundamental shear-wave is constant in this range, meaning it is a non-dispersive wave.

Therefore, by creating a shear-wave at the top of the ultrasonic viscometer setup and with the appropriate dimensions for the waveguide such that the frequency thickness product is between 0 - 1.5 [MHz·mm], the attenuation of the shear-wave in the waveguide will be solely due to the viscosity of the fluid in which it is immersed.

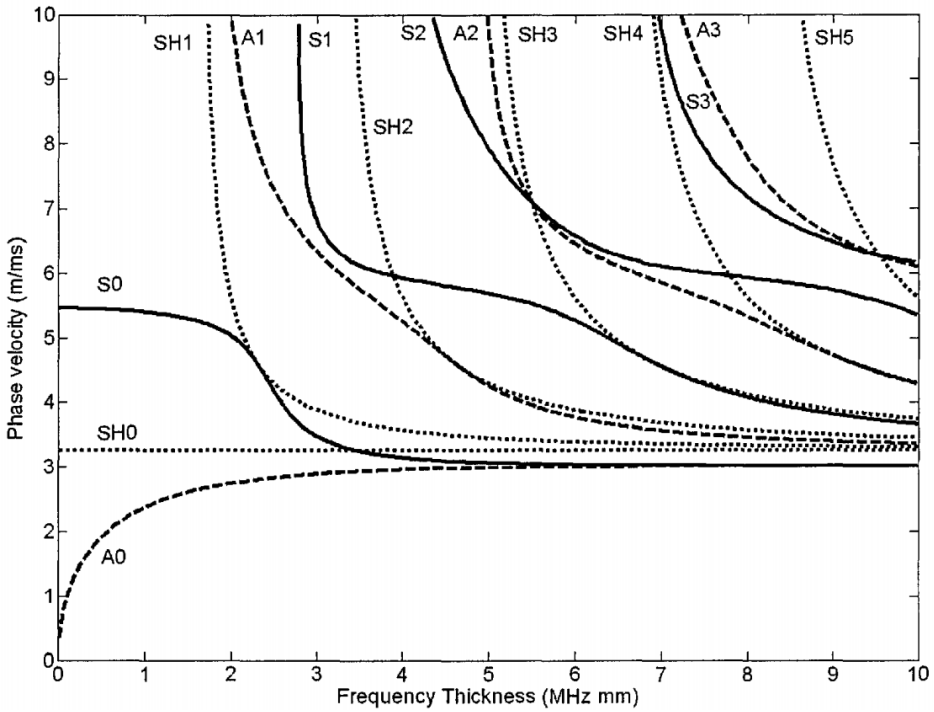

Figure 2.1: Phase velocity dispersion curves as a function of the frequency-thickness product for a steel plate with SH's describing the shear-wave modes, the A's describing the flexural wave modes and the S's the compressional wave modes [10].

2.2 Shear-wave in fluid

The second wave (II) used in this research is a shear-wave in a fluid resulting from the oscillating boundary of the waveguide. To describe the motion of a viscous fluid, the Navier-Stokes momentum equations can be used. By using the constraints and boundary conditions specific to a periodically oscillatory wall in the presence of a Power-law fluids, a specific governing momentum equation can be found. This equation is necessary since it provides a solution for the velocity profile in the specified fluid and thus the energy loss due to that fluid at a specific location. In this way the energy loss of the shear-wave propagating through the waveguide immersed in a fluid can be coupled to the fluid characteristics. So, by solving the governing momentum equation using a numerical model the actual experimental setup can be mimicked and experiments can be performed.

In this research a waveguide with length L in the z-direction, thickness h in the y-direction and width W in the x-direction is immersed in a Power-law fluid, figure 1.2. The shear-wave initiated at the top of the waveguide propagates in the z-direction and oscillates with velocity v_x in the x-direction. The velocity profiles in v_y and v_z are zero and there is no convection. By assuming there are no pressure gradients and no gravitational effects in the x-direction the problem specific governing momentum equation becomes:

$$\rho_f \frac{\partial v_x}{\partial t} = -\frac{\partial \tau_{yx}}{\partial y} \tag{2.1}$$

where ρ_f is the density of the fluid and the term on the right hand side is the gradient in the y-direction of the shear-stress on the yx-plane. The initial and boundary conditions of this problem are:

$$\begin{aligned} \text{I.C.}: &\quad v_x(y,0) = 0 \\ \text{B.C.}: &\quad v_x(0,t) = B(z)\sin(\omega t) \quad ; \quad v_x(\infty,t) = 0 \end{aligned} \tag{2.2}$$

It is good to realise that this obtained reduced incompressible governing momentum equation is very similar to the momentum equation used in Stokes Second Problem.

As mentioned in section 2.1, by using a shear-wave through in a thin steel waveguide the attenuation of this wave will be solely due to the viscosity (shear friction) of the fluid the waveguide is immersed in. The theory behind this is treated in the next section.

2.3 Wave energy in waveguide

The next step is to relate the attenuation of the shear-wave to the rheology of the fluid theoretically, first given by Rohde [11]. Since this shear-wave is travelling on the surface of the waveguide the wave energy is lost by the shear friction at the solid/liquid interface. The amount of friction is determined by the material at this interface, in this case the fluid in which the waveguide is immersed. If the waveguide, see figure 1.2, has a width of W [m] along the x-axis and an infinitesimal length dz, then the energy loss $\Delta P(z,t)$ [W] at the surface is:

$$\Delta P_\tau(z,t) = -2 \cdot \tau_0(z,t) \cdot V_x(z,t) \cdot W \cdot dz \tag{2.3}$$

where there is a minus sign since its energy loss, a 2 because energy is lost at the both sides of the waveguide, the $\tau_0(z,t)$ [Pa] is the shear-stress at the solid/liquid interface which is determined by the type of fluid and V_x [m/s] is the local velocity of the shear-wave on the boundary polarised in the x-direction. The energy loss due the "immersion" in air can be neglected since the viscosity of air is much smaller than of a fluid. Also, the energy loss at the bottom of the waveguide where the shear-wave is reflected is neglected since this area is much smaller than the area at the sides of the plate $W \cdot h << W \cdot l$. This same argument is true in case of the surfaces at the side of the waveguide, if the amplitude would be big enough. Lastly, the internal friction is neglected because of the elasticity of the waveguide.

Now, by using the energy loss term in equation 2.3 the energy balance in the waveguide can be constructed and it looks as follows:

$$h \cdot W \cdot dz \cdot \frac{dE_w(z,t)}{dt} = P(z,t) - P(z+dz,t) + \Delta P_\tau(z,t) \tag{2.4}$$

where the left hand side of this energy balance gives the time rate of change of the wave energy density $E_w(z,t)$ [J/m^3], the first and second term on the right hand side give the energy difference over a distance dz in the waveguide and the last term on the right hand side gives energy loss due to friction. This equation is developed in order to relate the attenuation of the shear-wave in the waveguide to the rheology of the fluid of interest and this attenuation is a time-averaged value of the energy loss of the shear wave travelling through the immersed waveguide. Therefore, the time-average is taken of the energy balance equation, which gives the following expression:

$$\frac{1}{T}\int_T h \cdot \frac{dE_w(z,t)}{dt}dt' = \frac{1}{T}\int_T \frac{P(z,t) - P(z+dz,t)}{W \cdot dz}dt' + \frac{1}{T}\int_T \frac{\Delta P_\tau(z,t)}{W \cdot dz}dt' \tag{2.5}$$

By realising that the energy dissipation per wave period is very small, there is assumed that the system is quasi-stationary. This implies that the integral over one period of the time rate of change of the wave energy density is zero. This results in:

$$\frac{1}{T}\int_T \frac{P(z+dz,t) - P(z,t)}{W \cdot dz}dt' = \frac{1}{T}\int_T \frac{\Delta P_\tau(z,t)}{W \cdot dz}dt' \tag{2.6}$$

The left hand side of this equation can be written as the time-averaged integral over the spatial derivative of the wave energy in the waveguide. According to *Leibniz's Integral Rule* because the integration boundaries are constants, differentiation and integration are interchangeable:

$$\frac{1}{T}\int_T \frac{P(z+dz,t) - P(z,t)}{W \cdot dz}dt' = \frac{1}{T}\int_T \frac{dP(z,t)}{W \cdot dz}dt' = \frac{d}{dz}\left(\frac{1}{T}\int_T \frac{P(z,t)}{W}dt'\right) \tag{2.7}$$

The resulting integral describes the time-averaged power of a sinusoidal wave per unit length and this can be expressed in its amplitude $A(z)$ [m] in the following way:

$$\frac{d}{dz}\left(\frac{1}{T}\int_T \frac{P(z,t)}{W}dt'\right) = \frac{d}{dz}\left(\frac{1}{2}\rho_s c_s h \cdot \omega^2 A^2(z)\right) = \frac{d}{dz}\left(\frac{1}{2}\rho_s c_s h \cdot B^2(z)\right) \tag{2.8}$$

where $B(z) \equiv -A(z) \cdot \omega$ is the velocity amplitude [m/s], ω [s^{-1}] is the frequency of the wave, ρ_s [kg/m^3] is the density of the waveguide and c_s [m/s] is shear-wave speed in the waveguide. By combining the result of equation 2.8 with equations 2.3 and 2.6, the quasi-stationary energy equation looks like:

$$\frac{d}{dz}\left(\frac{1}{2}\rho_s c_s h B^2(z)\right) = \frac{1}{T}\int_T -2 \cdot \tau_0(z,t) \cdot V_x(z,t)dt' \tag{2.9}$$

After rewriting, *the general energy wave equation of the ultrasonic waveguide viscometer* is obtained:

$$B(z)\frac{dB(z)}{dz} = \frac{1}{\rho_s c_s h} \cdot \frac{1}{T}\int_T -2 \cdot \tau_0(z,t) \cdot V_x(z,t)dt' \tag{2.10}$$

To solve this equation an expression needs to be found for the local velocity of the shear-wave on the boundary V_x and the shear-stress on the boundary τ_0.

The velocity of the shear-wave on the boundary V_x is initiated by the transducer at the top of the waveguide. This transducer creates the following deformation in the waveguide:

$$U_x(z,t) = A(z) \cdot \sin(kz - \omega t) \tag{2.11}$$

where $A(z)$ is the amplitude of the shear-wave [m], z is the position along the waveguide [m], k the wavenumber [m^{-1}] and ω the frequency [s^{-1}]. By taking the time derivative of equation 2.11 the local velocity is obtain:

$$\frac{dU_x(z,t)}{dt} = V_x(z,t) = -A(z) \cdot \omega \cdot \cos(kz - \omega t) = B(z) \cdot \cos(kz - \omega t) \tag{2.12}$$

where, again, $B(z) \equiv -A(z) \cdot \omega$ is the velocity amplitude [m/s].

Lastly, an expression of the shear-stress on the boundary τ_0 needs to be found. This is not trivial, since τ_0 reacts differently to a changing shear-rate on the boundary for different types of fluids. The two types of fluids that will be used in this research are Newtonian fluids and Power-law fluids. The differences in shear-stress will be treated in the following section with the goal of using this result for further evaluation of obtained energy wave equation 2.10.

2.4 Fluid rheology

As discussed in the previous section, the τ_0 in the energy wave equation 2.10 refers to the shear-stress due to viscous forces which cause energy loss of the shear-waves on the interface of the waveguide. This energy loss is transferred to the shear-wave in the fluid perpendicular to the waveguide, see figure 2.2. One can image that the magnitude of this new shear-wave depends on the properties of fluid; the more viscous the fluid, the larger the shear-stress and thus the more energy is lost in the fluid. However, in some fluids the shear-stress is also influenced by the time rate of change of the shear deformation in the fluid, the local velocity gradient, also known as the shear-rate, defined as: $\dot{\gamma} = \frac{\partial u_i}{\partial x_j} + \frac{\partial u_j}{\partial x_i}$ [m^{-1}].

The change in flow characteristics of a fluid caused by applied force is called the rheology of a fluid. If the viscosity of a fluid is independent of the shear-rate, the fluid is called Newtonian. The expression of the shear-stress in a Newtonian fluid is given by:

$$\tau_N = -\mu_0 \cdot \dot{\gamma} \tag{2.13}$$

where μ_0 [Pa·s] is the constant dynamic viscosity. However, there are also fluids of which the viscosity is affected by the applied force, such fluids are called non-Newtonian. There are various different types of non-Newtonian fluids such as: Power-Law, Bingham and Casson

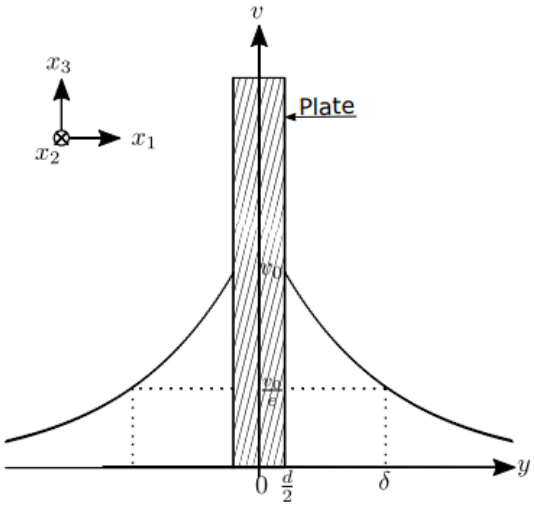

Figure 2.2: Schematic figure [12] of absolute velocity amplitude v attenuation of shear-wave in a fluid where δ represents the wave penetration depth, also known as the *viscous skin depth*. Note that this figure is not to scale, since $\delta \ll v$.

fluids. In this research the Power-law fluid is investigated. In case of Power-law fluids one does not have an absolute constant viscosity, but an apparent viscosity, defined as [15]:

$$\mu_{app}(\dot{\gamma}) = K_m \cdot |\dot{\gamma}|^{m-1} \tag{2.14}$$

where m [-] is called the *flow index* and K_m is called the *consistency index* [Pa·s^m]. These two parameters are called the *rheological properties* of a fluid and they characterise the behaviour of Power-law fluids. The full shear-stress expression of Power-law fluids, also known as the *Ostwald-De Waele model*, is:

$$\tau_{PL} = -\mu_{app}(\dot{\gamma}) \cdot \dot{\gamma} = -K_m \cdot |\dot{\gamma}|^{m-1} \cdot \dot{\gamma} \tag{2.15}$$

If $m = 1$ is used in this expression the Newtonian solution for viscosity is retrieved since $K_1 = \mu_0$, which means that Newtonian fluids are a special case of Power-law fluids. In the situation where $m < 1$ the fluids are called *shear-thinning* fluids because if the shear-rate increases the apparent viscosity decreases. The other way around, when $m > 1$, is called *shear-thickening* where the viscosity increases with increasing shear-rate. Figure 2.3 depicts the shear-stress/shear-rate relation for a Newtonian fluid and for an assembly of non-Newtonian fluids.

Looking back at the general energy equation 2.10 the corresponding shear-stress relations will be used in order to solve this equation in case of a Newtonian fluid and a Power-law fluid. An expression needs to be found for the shear-rate of different fluids. In the next sections the solution of the energy equation for Newtonian and Power-law fluids will be treated.

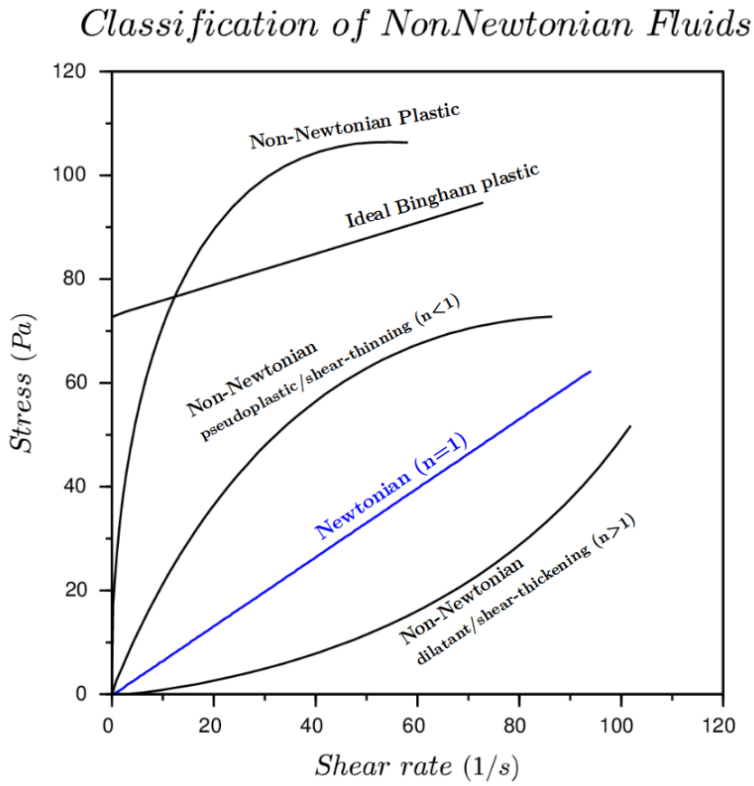

Figure 2.3: A shear-rate versus shear-stress plot for Newtonian and non-Newtonian fluids. Note that in this figure n is used as flow index parameter [16].

2.5 Energy equation for Newtonian fluid

In this section a solution is given to the general energy equation 2.10 for Newtonian fluids, first given by Rohde [11]. In this solution the Newtonian expression for the shear-stress, equation 2.13, will be used, but an expression for the shear-rate in a Newtonian fluid is still needed. Note that the *shear-stress on the boundary* needs is to be used in this solution, therefore also the *shear-rate on the boundary* needs to be used, thus $\dot{\gamma}_0$. As mentioned earlier in this chapter the shear-rate is the local velocity gradient in the fluid. This means that the shear-stress of a Newtonian fluid can be solved if the velocity profile of the shear-wave can be found.

This velocity profile is found analytically as a part of *Stokes Second Problem* [17]. The Stokes Second Problem describes an infinitely long boundary layer, a plate, which oscillates periodically and creates a velocity profile in the fluid. In the viscometer setup used in this research, see figure 1.2, the waveguide oscillates periodically in the x-direction at $y = 0$ (at a position z) since the fluid domain is $y > 0$. According to the solution to Stokes Second Problem the velocity profile can be written as:

$$v_x(y,t) = A \cdot \exp\left(-\frac{y}{\delta_N}\right) \cdot \cos\left(\omega t - \frac{y}{\delta_N}\right) \tag{2.16}$$

where A is the initial amplitude of the wave, $\delta_N \equiv \sqrt{\frac{2\mu_0}{\rho_f \omega}}$ [m] is the viscous skin depth of the shear-wave in the fluid with μ_0 and ρ_f the viscosity and density of the fluid. If this velocity profile will be used in the determination of the shear-rate, there needs to be adjusted for the fact that in this research not the entire plate is oscillating and that there should be a dependency on z in the velocity profile, since $A(z)$. Looking at the order of magnitude difference between the change in v_x in the y-direction ($\frac{dv_x}{dy} \approx \frac{v_x}{\delta_N}$) and the change in v_x in the z-direction ($\frac{dv_x}{dz} \approx \frac{v_x}{\lambda}$), where λ is the wavelength of shear-wave in the waveguide, it is noticed that:

$$\frac{dv_x}{dy} \gg \frac{dv_x}{dz} \tag{2.17}$$

since δ_N is $\mathcal{O}(10^{-6})$ (in case of water) and λ is $\mathcal{O}(10^{-3})$ because the frequency is in the MHz-range. More descriptively, equation 2.17 entails that at a position z the change in v_x is much more significant in the y-direction than the change in v_x in the z-direction in this setup. Therefore, the velocity profile of the shear-wave can be written as:

$$v_x(y,z,t) = A(z) \cdot \exp\left(-\frac{y}{\delta_N}\right) \cdot \cos\left(kz - \omega t - \frac{y}{\delta_N}\right) \tag{2.18}$$

where k is the wavenumber [m^{-1}]. By taking the gradient of this shear-wave velocity at the boundary, $y = 0$:

$$\frac{dv_x}{dy}\Big|_{y=0} = \frac{B(z)}{\delta_N}\cos(kz - \omega t) + \frac{B(z)}{\delta_N}\sin(kz - \omega t) = \sqrt{2}\frac{B(z)}{\delta_N}\cos(kz - \omega t - \pi/4) \tag{2.19}$$

the *shear-rate on the boundary of a Newtonian fluid* is obtained:

$$\dot{\gamma}_{0,N} = \sqrt{2}\frac{B(z)}{\delta_N}\cos(kz - \omega t - \pi/4) \tag{2.20}$$

This shear-rate on the boundary can now be used to solve the shear-stress on the boundary in a Newtonian fluid, equation 2.13. The expression for shear-stress becomes:

$$\tau_0(z,t) = -\mu_0 \cdot \dot{\gamma}|_{y=0} = -\mu_0 \cdot \frac{dv_x}{dy}|_{y=0} = -\mu_0 \cdot \sqrt{2}\frac{B(z)}{\delta_N} \cdot \cos\left(kz - \omega t - \frac{\pi}{4}\right) \tag{2.21}$$

Finally, by using this expression for the shear-stress and the velocity profile on the boundary, equation 2.12, a solution to the energy equation 2.10 for a Newtonian fluid can be given:

$$B(z)\frac{B(z)}{dz} = \frac{1}{\rho_s c_s h} \cdot \frac{1}{T}\int_T -\mu_0 \cdot 2 \cdot \sqrt{2}\frac{B(z)}{\delta_N} \cdot \cos\left(kz - \omega t - \frac{\pi}{4}\right) \cdot B(z) \cdot \cos(kz - \omega t)dt' \tag{2.22}$$

All the terms, except for cosines, can be taken out of the integral since they do not depend

on time, after which the integral can be solved by again using the identity: $\sin(x)+\cos(x) = \sqrt{2}\cos(x-\pi/4)$, giving:

$$\frac{1}{T}\int_T \cos\Big(kz-\omega t-\frac{\pi}{4}\Big)\cdot\cos(kz-\omega t)dt' = \frac{1}{2\sqrt{2}} \tag{2.23}$$

The resulting expression can be rewritten to obtain the following differential equation:

$$\frac{dB(z)}{dz} = -\frac{\mu_0}{\delta_N \rho_s c_s h}B(z) \tag{2.24}$$

This makes the *solution of the wave energy in the ultrasonic waveguide in a Newtonian fluid*:

$$B(z) = B(0)\cdot\exp(-\alpha\cdot z) \quad \text{with} \quad \alpha = \frac{\mu_0}{\delta_N\rho_s c_s h} = \frac{1}{\rho_s c_s h}\sqrt{\frac{\rho_f\omega\mu_0}{2}} \tag{2.25}$$

where α is called the *attenuation coefficient* [1/m] and $B_0 = B(0)$ is the *initial velocity amplitude* [m/s]. Lastly, by combining two solutions of this equation for two different immersion depths l_1 and l_2, note that $z - z_0 = 2l$, an expression is obtained to find the attenuation coefficient experimentally:

$$\frac{B(l_1)}{B(l_2)} = \exp(-\alpha(2l_1-2l_2)) \tag{2.26}$$

giving the expression of finding the attenuation coefficient experimentally:

$$\alpha = -\frac{1}{2}\cdot\frac{1}{l_1-l_2}\ln\left(\frac{B(l_1)}{B(l_2)}\right) \tag{2.27}$$

2.6 Energy equation for Power-law fluid

Similar to the previous section where a theoretical and an experimental solution to the attenuation coefficient can be found to determine the viscosity of the Newtonian fluid, the same approach is used to determine the rheological properties, namely the flow index and consistency index, of a Power-law fluid, first given by Rohde [11]. Therefore the shear-stress on the boundary in the general energy equation 2.10 needs to be solved for a Power-law fluid:

$$\tau_{0,PL} = -K_m\cdot|\dot{\gamma}_{0,PL}|^{m-1}\cdot\dot{\gamma}_{0,PL} \tag{2.28}$$

This shear-stress can be solved if an expression of the shear-rate on the boundary $\dot{\gamma}_{0,PL}$ is known and therefore the velocity profile in a Power-law fluid needs to be known analytically to find the velocity gradient on the boundary:

$$\dot{\gamma}_{0,PL} = \frac{d}{dy}(v_{x,PL})|_{y=0} \tag{2.29}$$

However, an analytical expression of the velocity profile of a shear-wave in a Power-law fluid does *not* exist in the same way as in the Newtonian situation where Stokes solution exists. This leads to following question:

* Can a solution be found of the shear-rate on the boundary between a oscillating plate and a Power-law fluid without a solution to the velocity profile?

This question seems a better starting point since only the solution of the shear-rate on the boundary needs to known, which already puts a constraint on an otherwise more general problem. In this section three different expressions of the shear-rate on the boundary in a Power-law fluid ($\dot{\gamma}_{0,PL}$) are proposed. Section 2.6.2 and 2.6.3 treat the theory behind two shear-rates on the boundary based on a paper of Ai & Vafai [13], which is discussed in section 2.6.1. Section 2.6.4 proposes an alternative expression of the shear-rate not based on the result of Ai & Vafai.

2.6.1 Dimensionless velocity profiles of Ai & Vafai

There exists a result of Ai & Vafai [13] which gives an insight in what the shear-rate on the boundary in Power-law fluid created by an oscillating boundary layer might look like. Figure 2.4 shows the dimensionless velocity profiles at various times τ created by an oscillating wall with velocity $u_w = u_0 \sin(\tau)$ at $\eta = 0$. In this study the following definitions are used: $\tau = \hat{t}$, $u_w = v_x$, $u_0 = v_0$ and $\eta = \hat{y}$, where the hats denote non-dimensionality. The velocity profiles for three flow indices, $m = 0.5$, $m = 1$, $m = 1.5$, in figure 2.4 are created by using a dimensionless governing momentum equation, obtained by combining the momentum equation 2.1 with the dimensionless parameters from Ai & Vafai [13]:

$$\hat{t} = \omega t, \quad \hat{y} = y\sqrt{\frac{\rho_f \omega}{\mu_0}} \quad \text{and} \quad \hat{v}_x = \frac{v_x}{v_0} \tag{2.30}$$

where $\hat{t}$ is the dimensionless time, $\hat{y}$ the dimensionless y and $\hat{v}_x$ the dimensionless velocity, and v_0, ω, ρ_f and μ_0 are the reference parameters of velocity, frequency, density and viscosity respectively [13]. The dimensionless LHS of momentum equation 2.1 is given as [13]:

$$\frac{\partial v_x}{\partial t} = v_0 \cdot \omega \cdot \frac{\partial \hat{v}_x}{\partial \hat{t}} \tag{2.31}$$

The next step is to make the RHS of momentum equation 2.1 dimensionless. The shear-stress term is evaluated separately for the sake of clarity before combining it with the dimensionless gradient [13]:

$$\tau_{yx} = -K_m \cdot \left|\frac{\partial v_x}{\partial y}\right|^{m-1} \cdot \frac{\partial v_x}{\partial y} = -K_m \cdot \left[\left(\frac{\omega \rho_f}{\mu_0}\right)^{1/2} \cdot v_0\right]^m \cdot \left|\frac{\partial \hat{v}_x}{\partial \hat{y}}\right|^{m-1} \cdot \frac{\partial \hat{v}_x}{\partial \hat{y}} \tag{2.32}$$

$$\frac{\partial \tau_{yx}}{\partial y} = -K_m \cdot \left[\left(\frac{\omega \rho_f}{\mu_0}\right)^{1/2} \cdot v_0\right]^m \cdot \left(\frac{\omega \rho_f}{\mu_0}\right)^{1/2} \cdot \frac{\partial \hat{\tau}_{yx}}{\partial \hat{y}} \tag{2.33}$$

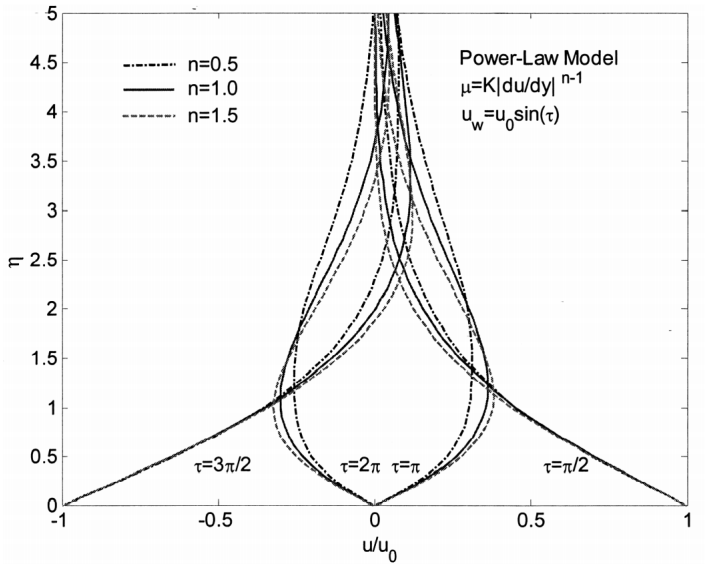

Figure 2.4: Dimensionless velocity profiles in a Power-law model for three different flow indices at four time intervals created by an oscillating wall at $\eta = 0$ from research of Ai & Vafai [13].

Combining the result of equation 2.31 and equation 2.33 in equation 2.1, the dimensionless governing momentum equation is obtained [13]:

$$\frac{\partial \hat{v}_x}{\partial \hat{t}} = -\kappa \cdot \frac{\partial \hat{\tau}_{yx}}{\partial \hat{y}} \quad \text{with} \quad \kappa = \frac{K_m}{\mu_0} \cdot \left(\frac{\omega \rho_f}{\mu_0}\right)^{\frac{m-1}{2}} \cdot v_0^{m-1} \tag{2.34}$$

with κ [-] being a dimensionless constant defined by the reference parameters of equation 2.30. Note that the flow index $m = 1$, which implies $K_{m=1} = \mu_0$, gives the Newtonian solution where $\kappa = 1[-]$.

2.6.2 Proposed shear-rate I

The proposed shear-rate on the boundary of a Power-law fluid ($\dot{\gamma}_{0,PL}$) in this section is based on the result of figure 2.4, first suggested by Rohde [11]. The importance of this figure resides in the fact that it shows the dimensionless velocity profiles for different flow indices, $m = 0.5$ (shear-thinning), $m = 1$ (Newtonian) and $m = 1.5$ (shear-thickening) very close to the boundary with the oscillating interface. Therefore, this figure also gives information about the shear-rate very close to the boundary for different flow indices and it seems that the shear-rates for the flow indices $m = 0.5$, $m = 1$ and $m = 1.5$ very close to the boundary are equal. The idea by Rohde [11] is:

If the shear-rate very close to the boundary of an oscillating plate in a Power-law fluid ($m \neq 1$) *is independent of flow index m, is it possible to use the solution of the shear-rate on the boundary in a Newtonian fluid* ($m = 1$) *instead, since this is known analytically*?

Furthermore, this independence of the flow index m would imply that the condition on the consistency index becomes: $K_m = K_1 = \mu_0$. Mathematically, this idea proposed by Rohde [11] is given as:

$$\frac{d}{d\hat{y}}(\hat{v}_{x,PL})|_{\hat{y}=0} = \frac{d}{d\hat{y}}(\hat{v}_{x,N})|_{\hat{y}=0} \tag{2.35}$$

where the LHS of this equation gives the dimensionless shear-rate on the boundary in a Power-law fluid and the RHS gives the dimensionless shear-rate on the boundary in a Newtonian fluid. Equation 2.35 is valid in the dimensionless case since the result of Ai & Vafai is dimensionless, but the dimensional expression of the shear-rate on the boundary is needed in equation 2.29. By using the dimensionless definitions for $\hat{y}$ and $\hat{v}_x$ of equation 2.30 in equation 2.35 it can be transformed to the dimensional expression. Since $\hat{y}$ and $\hat{v}_x$ are not a function of m, the dimensional expression of equation 2.35 is:

$$\frac{d}{dy}(v_{x,PL})|_{y=0} = \frac{d}{dy}(v_{x,N})|_{y=0} \tag{2.36}$$

where the LHS is the shear-rate on the boundary in a Power-law fluid ($\gamma_{0,PL}$) and the RHS of this equation is equal to Newtonian shear-rate on the boundary ($\gamma_{0,N}$) given by equation 2.20 with the condition that $K_m = \mu_0$. This results in the *first proposed shear-rate on the boundary of a Power-law fluid*:

$$\dot{\gamma}_{0,PL} = \sqrt{2}\frac{B(z)}{\delta_{PL}}\cos(kz - \omega t - \pi/4) \quad \text{with} \quad \delta_{PL} = \sqrt{\frac{2K_m}{\rho_f \omega}} \tag{2.37}$$

By using this expression of the shear-rate, the shear-stress of equation 2.28 can be found in order to solve the general energy equation 2.10 for a Power-law fluid. This results in the following expression for the energy equation:

$$B(z)\frac{B(z)}{dz} = \frac{-2K_m}{\rho_s c_s h}\left(\sqrt{2}\frac{B(z)}{\delta_{PL}}\right)^m B(z)\cdot P_3(m) \tag{2.38}$$

where the term $P_3(m)$ containing the integral is written as:

$$P_3(m) = \frac{1}{T}\int_T \left|\cos\Big(kz - \omega t - \frac{\pi}{4}\Big)\right|^{m-1} \cdot \cos\Big(kz - \omega t - \frac{\pi}{4}\Big)\cdot\cos(kz - \omega t)dt' \tag{2.39}$$

By realising that the identity in the integral is periodic over a period π and by using the substitution $\xi = kz - \omega t$, this integral can be solved by using polynomial approximation: $P_3(m) \approx 0.00630863m^3 + 0.0399466m^2 - 0.129211m + 0.448619$ which only depends on the flow index m. This results in the following differential equation:

$$\frac{dB(z)}{dz} = \frac{-2K_m P_3(m)}{\rho_s c_s h}\left(\frac{\sqrt{2}}{\delta_{PL}}\right)^m B(z)^m \tag{2.40}$$

This equation can be solved for $m \neq 1$ which gives the final solution:

$$B(l) = \left(B_0^{1-m} + 2 \cdot (1-m) \cdot \alpha_m \cdot l\right)^{(1/1-m)} \tag{2.41}$$

$$\alpha_m(\omega) = -2\frac{K_m P_3(m)}{\rho_s c_s h} \cdot \left(\frac{\sqrt{2}}{\delta_{PL}}\right)^m = -2\frac{P_3(m)}{\rho_s c_s h} \cdot (\rho_f \omega)^{m/2} \cdot K_m^{\frac{2-m}{2}} \tag{2.42}$$

Note that $(z-z_0)$ is the entire distance travelled by the shear-wave in the waveguide, therefore the immersion depth l is defined as: $l = \frac{(z-z_0)}{2}$. The challenge that still remains is how to find the rheological properties m and K_m experimentally using this solution. The methods used to find these properties using equation 2.41 are discussed in the next chapter.

2.6.3 Proposed shear-rate II

This section treats the theory of a newly proposed shear-rate on the boundary in a Power-law fluid, different from equation 2.37, and the solution to the energy equation 2.10. In figure 2.4 it can be seen that the dimensionless velocity profiles for the flow indices $m = 0.5$, $m = 1$ and $m = 1.5$ very close to the boundary are almost equal and the corresponding shear-rates very close to the boundary also appear to be equal to each other. The new suggested reason behind this is that the shear-rates on the boundary for different flow indices are equal if their corresponding values for dimensionless constant κ are equal, given in equation 2.34. Therefore, the idea is:

If the shear-rates on the boundary of a Power-law fluid ($m \neq 1$, K_m) are equal if their corresponding dimensionless constants κ are equal, is it possible to use the solution of the shear-rate on the boundary in a Newtonian fluid ($m = 1$, $K_{m=1} = \mu_0$) instead, since this is known analytically, under the condition of constant κ?

Expressing this idea mathematically results in the following equation:

$$\frac{d}{d\hat{y}}(\hat{v}_{x,m_1})|_{\hat{y}=0} = \frac{d}{d\hat{y}}(\hat{v}_{x,m_2})|_{\hat{y}=0} \quad \text{if} \quad \kappa_{m_1} = \kappa_{m_2} \tag{2.43}$$

where the dimensionless shear-rates for different flow indices m_1 and m_2 are equal only if the condition of constant κ is met. The condition of constant κ is expressed as:

$$\frac{K_{m_1}}{\mu_0} \cdot \left(\frac{\omega \rho_f}{\mu_0}\right)^{\frac{m_1-1}{2}} \cdot v_0^{m_1-1} = \kappa = \frac{K_{m_2}}{\mu_0} \cdot \left(\frac{\omega \rho_f}{\mu_0}\right)^{\frac{m_2-1}{2}} \cdot v_0^{m_2-1} \tag{2.44}$$

thereby using equation 2.34 and two sets of rheological properties, namely (m_1, K_{m_1}) and (m_2, K_{m_2}). The terms v_0, ω, ρ_f and μ_0 are the reference parameters from equation 2.30. In case of a Newtonian fluid with the rheological properties ($m_2 = 1$, $K_{m_2} = \mu_0$) in equation 2.44, giving value of $\kappa = 1$, and with a Power-law fluid ($m_1 = m$, $K_{m_1} = K_m$), equation 2.44 is rewritten as:

$$\frac{K_m}{\mu_0} \cdot \left(\frac{\omega \rho_f}{\mu_0}\right)^{\frac{m-1}{2}} \cdot v_0^{m-1} = \kappa = 1 \quad \rightarrow \quad \mu_0 = K_m^{\frac{2}{m+1}} \cdot \left(\omega \cdot \rho_f \cdot v_0^2\right)^{\frac{m-1}{m+1}} \tag{2.45}$$

such that the condition of constant κ between a Newtonian fluid and a Power-law fluid is given to the Newtonian viscosity μ_0. The resulting expression for equal dimensionless shear-rate on the boundary in a Power-law fluid and Newtonian fluid is given by:

$$\frac{d}{d\hat{y}}(\hat{v}_{x,PL})|_{\hat{y}=0} = \frac{d}{d\hat{y}}(\hat{v}_{x,N})|_{\hat{y}=0} \quad \text{if} \quad \mu_0 = K_m^{\frac{2}{m+1}} \cdot \left(\omega \cdot \rho_f \cdot v_0^2\right)^{\frac{m-1}{m+1}} \tag{2.46}$$

This equation 2.46 is valid for dimensionless shear-rates on the boundary, but the dimensional expression of the shear-rate on the boundary is needed to find a solution to the energy equation 2.10. By using the reference parameters for $\hat{y}$ and $\hat{v}_x$ of equation 2.30 in equation 2.46 it can be transformed to the dimensional expression. Since $\hat{y}$ and $\hat{v}_x$ are not a function of m, the dimensional expression of equation 2.46 becomes:

$$\frac{d}{dy}(v_{x,PL})|_{y=0} = \frac{d}{dy}(v_{x,N})|_{y=0} \quad \text{if} \quad \mu_0 = K_m^{\frac{2}{m+1}} \cdot \left(\omega \cdot \rho_f \cdot v_0^2\right)^{\frac{m-1}{m+1}} \tag{2.47}$$

where the LHS is the shear-rate on the boundary in a Power-law fluid ($\dot{\gamma}_{0,PL}$) and the RHS of this equation is equal to Newtonian shear-rate on the boundary ($\dot{\gamma}_{0,N}$) given by equation 2.20. This results in the *second proposed shear-rate on the boundary of a Power-law fluid*:

$$\dot{\gamma}_{0,PL} = \sqrt{2}\frac{B(z)}{\sqrt{\frac{2\mu_0}{\rho_f \omega}}}\cos(kz - \omega t - \pi/4) \quad \text{with} \quad \mu_0 = K_m^{\frac{2}{m+1}} \cdot \left(\omega \cdot \rho_f \cdot v_0^2\right)^{\frac{m-1}{m+1}} \tag{2.48}$$

This solution to the shear-rate on the boundary in a Power-law fluid is used to find the shear-stress of equation 2.28 in order to solve the general energy equation 2.10. This results in the following expression for the energy equation:

$$B(z)\frac{B(z)}{dz} = \frac{-2K_m}{\rho_s c_s h}\left(\sqrt{2}\frac{B(z)}{\sqrt{\frac{2\mu_0}{\rho_f \omega}}}\right)^m B(z) \cdot P_3(m) \quad \text{with} \quad \mu_0 = K_m^{\frac{2}{m+1}} \cdot \left(\omega \cdot \rho_f \cdot v_0^2\right)^{\frac{m-1}{m+1}} \tag{2.49}$$

where the term $P_3(m)$ is given by equation 2.39. Equation 2.49 can be solved for $m \neq 1$ which gives the final solution:

$$B(l) = \left(B_0^{1-m} + 2 \cdot (1-m) \cdot \alpha_s \cdot l\right)^{(1/1-m)} \tag{2.50}$$

$$\alpha_s(\omega) = -2\frac{P_3(m)}{\rho_s c_s h} \cdot (\rho_f \omega)^{\frac{m}{m+1}} \cdot B_0^{\frac{-m^2+m}{m+1}}(\omega) \cdot K_m^{\frac{1}{m+1}} \tag{2.51}$$

using that $v_0 = B_0$ are the same initial velocity amplitude and $l = \frac{(z-z_0)}{2}$. The methods used to find these properties using equation 2.50 are discussed in the next chapter.

2.6.4 Alternative expression of the shear-rate

This section treats the theory proposing a new expression of the shear-rate on the boundary in a Power-law fluid ($\dot{\gamma}_{0,PL}$) *not* based on the result of figure 2.4 of Ai & Vafai.

Since the solution to the shear-rate in a Newtonian fluid ($\dot{\gamma}_{0,N}$) is known analytically, equation 2.20, the earlier mentioned suggestion to use this Newtonian expression as a solution to the shear-rate in a Power-law fluid remains. However, ($\dot{\gamma}_{0,N}$) contains the constant dynamic viscosity term μ_0, but Power-law fluids do not have a constant viscosity, these fluids have an apparent viscosity $\mu_{app}(\dot{\gamma})$, equation 2.14. This results in the following idea:

Is it possible to use the solution of the shear-rate on the boundary in a Newtonian fluid ($m = 1$) as solution to the shear-rate on the boundary in a Power-law fluid ($m \neq 1$) if the constant dynamic viscosity term μ_0 is replaced with the apparent viscosity term $\mu_{app}(\dot{\gamma})$?

The apparent viscosity $\mu_{app}(\dot{\gamma})$ is a function of the shear-rate, which needs to be obtained in the first place. Therefore, the used solution to the apparent viscosity $\mu_{app}(\dot{\gamma})$ will be found numerically (Approach A) and an analytical suggestion of the apparent viscosity will be made (Approach B), both approaches are described in section 3.2.6 of the next chapter.

By having a solution to apparent viscosity, an expression of the shear-rate can be found. Using this newly proposed idea and by replacing the constant viscosity in equation 2.20 with the (now known) apparent viscosity $\mu_{app}(\dot{\gamma})$, the following proposed shear-rate on the boundary of a Power-law fluid is obtained:

$$\dot{\gamma}_{0,PL} = \sqrt{2}\frac{B(z)}{\delta_{PL}}\cos(kz - \omega t - \pi/4) \quad \text{with} \quad \delta_{PL} = \sqrt{\frac{2 \cdot \mu_{app}(\dot{\gamma})}{\rho_f \cdot \omega}} \tag{2.52}$$

This shear-rate on the boundary in a Power-law fluid is used to find the shear-stress of equation 2.28 in order to solve the general energy equation 2.10. This results in the following expression for the energy equation:

$$\frac{B(z)}{dz} = -2\frac{K_m}{\rho_s c_s h}\left(\frac{\rho_f \cdot \omega}{\mu_{app}(\dot{\gamma})}\right)^{m/2} \cdot P_3(m) \cdot B(z)^m \tag{2.53}$$

where the term $P_3(m)$ is given by equation 2.39. Equation 2.53 can be solved for $m \neq 1$ which gives the final solution:

$$B(l) = \left(B_0^{1-m} + 2 \cdot (1-m) \cdot \alpha_r \cdot l\right)^{(1/1-m)} \tag{2.54}$$

$$\alpha_r(\omega) = -2\frac{K_m}{\rho_s c_s h}\left(\frac{\rho_f \cdot \omega}{\mu_{app}(\dot{\gamma})}\right)^{m/2} \cdot P_3(m) \tag{2.55}$$

where the immersion depth l is defined as: $l = \frac{(z-z_0)}{2}$. The methods used to find these properties using equation 2.54 are discussed in the next chapter.

Chapter 3

Methods

The grand objective of this study is to find the rheological properties of Power-law fluids using a shear-wave through a waveguide plate dipped in that fluid. This chapter describes all the methods used to obtain the results provided in chapter 4.

In this study a numerical model is used to mimic a real experimental ultrasonic waveguide setup. Therefore, the first part of this chapter treats the details of this model and its validation by comparing it with benchmark cases.

The second part of this chapter focuses on developing methods to obtain the rheological properties m and K_m using the numerically created amplitude measurements of the numerical model and the three analytical solutions to the energy equation 2.42, 2.50 and 2.54, and their corresponding attenuation coefficients α, equations 2.42, 2.51 and 2.55.

3.1 The numerical viscometer

In the previous chapter the research specific governing momentum equation 2.1 is derived. The velocity profiles in specified Power-law fluids need to be solved for in order to correctly model the attenuated wave in the waveguide. To evaluate this equation computationally a finite difference scheme will be utilised which discretises this momentum equation. By making use of a coupling constant the energy loss related to the created velocity profile will be linked to the loss of energy in the waveguide.

3.1.1 Discrete notation

Discretisation is the approach to divide a continuous function in discrete parts in order to solve that function computationally. There are various different methods to discretise a problem and the choice of the used method is a balance between the characteristics of that problem, the amount of processing power available and accuracy. Although, it is good to realise that a numerical solution essentially should not influence the final established solution of a system of equations, it can only influence the trajectory on how this solution is found from an initial guess.

In the numerical model used in this study the functions that need to be discretised depend on the parameters t, y, z, which are time, the y-direction and the z-direction respectively. Recall that the y-direction is the domain of the fluid and the z-direction is along the surface of the waveguide. The following notation will be chosen:

$$f_{i,k}^{n} = f(y_i, z_k, t_n) \quad \text{with} \quad y_i = i\Delta y, \quad z_k = k\Delta z, \quad t_n = n\Delta t \tag{3.1}$$

where Δy, Δz, Δt are the discrete step sizes and i, k, n are the number of steps. Depending on which approximation technique will be used conditions must be placed on the size of some step sizes and the number of steps needed. The used numerical methods will be discussed next.

3.1.2 Finite difference methods

A broadly used numerical technique of approximating a derivative, in time (t) or space (x), is by using the Finite Difference Method (FDM), of which the most basic techniques are the Forward, Backward and Centered approximations [18]. These methods rely on the fact that the derivative of a function at a certain position is defined as the limit [19]:

$$f'(x) = \lim_{h \to 0} \frac{f(x+h) - f(x)}{h} \tag{3.2}$$

This approximation of the derivative becomes better the smaller h gets. In this case h is the distance between between two consecutive point of the function $f(x)$. However, h can never be zero so there always is a certain error when using this approximation. To say anything about this error the order of convergence of this approximation is investigated, therefore a Taylor expansion is performed on $f(x+h)$:

$$f(x+h) = f(x) + h \cdot f'(x) + \frac{h^2}{2!} \cdot f''(x) + h.o.t. \tag{3.3}$$

where the large part of the higher order terms (*h.o.t.*) are neglected since the power of h keeps increasing with these terms and thus its contribution to the solution almost completely vanishes when h is sufficiently small. If the Taylor expansion is rewritten into an expression for the derivative, it results in:

$$f'(x) = \frac{f(x+h) - f(x)}{h} - \frac{h}{2} \cdot f''(x) \tag{3.4}$$

This equation is known as the *Forward Finite Difference Method* [18] with first order convergence, since the error in this approximation drops by h. So the smaller h, the better the approximation. The first order *Backward Finite Difference Method* is similar to this result but instead the difference is taken between $f(x)$ and $f(x-h)$. By combining the Forward and Backward approach a new method of approximating a derivative is obtain:

$$f'(x) = \frac{f(x+h) - f(x-h)}{2h} - h^2 \cdot (h.o.t.). \tag{3.5}$$

This equation is known as the *Centered Finite Difference Method* [18] and contrary to the Forward and Backward method it has a second order of convergence. This is desirable since faster convergence means one can choose a larger h resulting in less points that need to be solved and thus less computation time to have an accurate result. This second order convergence is a feature which one wants to have in case of the Forward method as well. It is given by:

$$f'(x) = \frac{-3f(x) + 4f(x+h) - f(x+2h)}{2h} \tag{3.6}$$

and this equation is known as the *second order Forward Finite Difference Method* [19].

3.1.3 Discrete governing momentum equation

The governing momentum equation from equation 2.1 consists of the time derivative of the velocity profile polarised in the x-direction and of the spatial y-derivative of the shear-stress. Now, since the shear-stress of a Power-law fluid, described by equation 2.15, depends on the local velocity gradient, the governing momentum equation is a partial differential equation:

$$\rho_f \frac{\partial v_x}{\partial t} = -\frac{\partial \tau_{yx}}{\partial y} = -\frac{\partial}{\partial y}\left(-K_m \cdot \left|\frac{\partial v_x}{\partial y}\right|^{m-1} \cdot \frac{\partial v_x}{\partial y}\right) \tag{3.7}$$

In order to solve the governing momentum using finite difference methods it is necessary to know the initial and boundary conditions of the system. These conditions give insight in which methods are most suitable for which derivatives. The initial and boundary conditions of the velocity profile $v_x(y,t)$ in the fluid caused by the shear-wave on the waveguide are:

$$\begin{aligned} \text{I.C.}: &\quad v_x(y,0) = 0 \\ \text{B.C.}: &\quad v_x(0,t) = B_0 \sin(\omega t) \quad ; \quad v_x(\infty,t) = 0 \end{aligned} \tag{3.8}$$

The boundary condition gives the solution of velocity profile for every time step and the initial condition causes that the shear-stress is zero everywhere. Therefore, the time-derivative of the velocity profile will be approximated with the first order Forward Finite Difference method and the shear-stress will be approximated with the Centered Finite Difference method, as proposed by Borstlap [14]:

$$\rho_f \left(\frac{v_{i,k}^{n+1} - v_{i,k}^n}{\Delta t}\right) = -\left(\frac{\tau_{i+1,k}^n - \tau_{i-1,k}^n}{2\Delta y}\right) \tag{3.9}$$

and rewriting this equation gives an expression for the solution of the velocity profile in the next time step $n+1$:

$$v_{i,k}^{n+1} = v_{i,k}^{n} - \frac{\Delta t}{2\rho_f \Delta y} \cdot \left(\tau_{i+1,k}^{n} - \tau_{i-1,k}^{n}\right) \tag{3.10}$$

This expression is also known as the *Forward Time Centered Space* (FTCS) method and is often used with parabolic partial differential equations [20]. The FTCS method has a first order convergence in time and a second order convergence in space. So to maintain this second order convergence when expressing the spatial derivatives of the velocity profile in the shear-stress, the second order Forward Finite Difference Method of equation (3.6) is used. This results in:

$$\tau_{i,k}^{n} = -K_m \left| \frac{-3v_{i,k}^{n} + 4v_{i+1,k}^{n} - v_{i+2,k}^{n}}{2\Delta y} \right|^{m-1} \cdot \frac{-3v_{i,k}^{n} + 4v_{i+1,k}^{n} - v_{i+2,k}^{n}}{2\Delta y} \tag{3.11}$$

The shear-rate is of importance for the investigation of finding the rheological properties and can be numerically expressed as:

$$\dot{\gamma}_{i,k}^{n} = \frac{-3v_{i,k}^{n} + 4v_{i+1,k}^{n} - v_{i+2,k}^{n}}{2\Delta y} \tag{3.12}$$

Lastly, to solve equation 3.11, and thus equation 3.10, it must be checked if the shear-rate is larger than zero or smaller than zero to give a correct sign to the expression of the shear-stress. Therefore the following two equations are obtained:

$$\begin{aligned} &\text{If} \quad \dot{\gamma}_{i,k}^{n} > 0 \quad : \quad \tau_{i,k}^{n} = -K_m \cdot \left(\dot{\gamma}_{i,k}^{n}\right)^m = -K_m \cdot \left(\frac{-3v_{i,k}^{n} + 4v_{i+1,k}^{n} - v_{i+2,k}^{n}}{2\Delta y}\right)^m \\ &\text{If} \quad \dot{\gamma}_{i,k}^{n} < 0 \quad : \quad \tau_{i,k}^{n} = K_m \cdot \left(-\dot{\gamma}_{i,k}^{n}\right)^m = K_m \cdot \left(-\frac{-3v_{i,k}^{n} + 4v_{i+1,k}^{n} - v_{i+2,k}^{n}}{2\Delta y}\right)^m \end{aligned} \tag{3.13}$$

3.1.4 Coupling to wave in waveguide

The final step in mimicking the ultrasonic waveguide viscometer setup computationally is to link the energy loss in the fluid to the energy loss in the wave in the waveguide. Based on previous research [14] a constant I_X can be used that couples the energy loss due to viscous shear-stresses to the energy loss at a position z in the waveguide, which is given by:

$$I_X(z) = \frac{2}{T} \int_T X(z,t)dt \quad \text{with} \quad X(z,t) = \frac{1}{B(z)^{m+1}} \cdot \tau_0(z,t) \cdot v_{x,0}(z,t) \tag{3.14}$$

The idea behind this coupling constant is that by treating $B(z)$, the velocity amplitude at position z, as a scaling factor for the shear-stress on the boundary $\tau_0(z,t) \sim B(z)^m$ and the velocity on boundary $v_{x,0}(z,t) \sim B(z)$, one obtains a periodic relation $X(z,t)$ which is independent of the velocity amplitude. It is important to note that the remaining z-dependency in $X(z,t)$ refers to a shift in the periodic signal and *not* to the amplitude reduction as function of z, since has just been scaled out. Then, integrating $X(z,t)$ over one period gives

the same result independent of z, making $I_X(z) = constant$ for every value of z for a fixed frequency. This leads to the following simplification of energy equation 2.10:

$$\frac{dB(z)}{dz} = -B(z)^m \cdot \frac{I_X}{\rho_s c_s h} \tag{3.15}$$

This result is then used in the numerical model to link the energy loss due to viscous shear-stress to the energy loss in the waveguide. By approximating equation 3.15 using the Forward Finite Difference method, the equation becomes:

$$B^n_{i,k+1} = B^n_{i,k} - \frac{\Delta z}{\rho_s c_s h} \cdot I_X \cdot (B^n_{i,k})^m \tag{3.16}$$

The big advantage of using I_X is that it has to be calculated only once for one value of z which saves a considerable amount of computation time.

3.1.5 Dimensionless numerical model

In this research the discrete governing momentum equation 3.10 is also utilised in a dimensionless scenario. By using the dimensionless parameters described in equation 2.30 on the equations 3.10, 3.12 and 3.13, the dimensionless discrete governing momentum, the dimensionless numerical expression of the shear-rate and the dimensionless numerical expression of the shear-stress are obtained. The dimensionless discrete governing momentum is:

$$\hat{v}^{n+1}_{i,k} = \hat{v}^n_{i,k} - \kappa \cdot \frac{\Delta \hat{t}}{2 \cdot \Delta \hat{y}} \cdot \left(\hat{\tau}^n_{i+1,k} - \hat{\tau}^n_{i-1,k}\right) \tag{3.17}$$

where n, i and k are corresponding to the time, y and z respectively, $\Delta \hat{t}$ is the dimensionless time step and $\Delta \hat{y}$ the dimensionless step size in y. The dimensionless numerical expression of the shear-rate and the dimensionless numerical expression of the shear-stress are given by:

$$\hat{\dot{\gamma}}^n_{i,k} = \frac{-3\hat{v}^n_{i,k} + 4\hat{v}^n_{i+1,k} - \hat{v}^n_{i+2,k}}{2\Delta \hat{y}} \tag{3.18}$$

$$\begin{aligned} &\text{If} \quad \hat{\dot{\gamma}}^n_{i,k} > 0 \quad : \quad \hat{\tau}^n_{i,k} = -\left(\hat{\dot{\gamma}}^n_{i,k}\right)^m \\ &\text{If} \quad \hat{\dot{\gamma}}^n_{i,k} < 0 \quad : \quad \hat{\tau}^n_{i,k} = \left(-\hat{\dot{\gamma}}^n_{i,k}\right)^m \end{aligned} \tag{3.19}$$

The dimensionless constant κ shown in equation 3.17 is given by equation 2.34. The reference parameters for the density, viscosity frequency and amplitude used determine κ are given in table 3.1.

$\rho_f = 1000$ [kg/m^3]	$\mu_0 = 0.001$ [Pa·s]	$\omega = 2\pi \cdot 3.7$ [MHz]	$A(0) = 80$ [mm]

Table 3.1: Reference parameters used in dimensionless model. Note that $v_0 = A(0) \cdot \omega$.

3.1.6 Experimental setup waveguide and fluids

In this part the constants and parameters that will be used in the computations are shown. Table 3.2 shows the material properties of the stainless steel waveguide, the used range of frequencies and initial amplitude of the shear-wave in the waveguide. The material properties and initial amplitude are taken from the previous research of Rook [12]. The frequency range is chosen such that the frequency thickness product is smaller than 1.5 [MHz·mm], see section 2.1, and because this frequency range has the least power-loss in the waveguide as a function of the frequency according Rook [12].

In table 3.3 the rheological properties and densities of the Newtonian fluid *water* and the Power-law fluids *Ketchup*, *Soybean oil* and *Ethylene-Glycol* are shown.

ρ_s [kg/m^3]	c_s [m/s]	h [mm]	W [m]	L [m]	f [MHz]	$A(0)$ [mm]
7876	3083	0.202	0.0802	0.2035	3.3-4.3	80

Table 3.2: Waveguide parameters used in numerical model with ρ_s, c_s, h, W and L being the density, shear-wave speed, thickness, width and length of the steel waveguide respectively. Note that initial velocity amplitude $v_0 = A(0) \cdot \omega$ is a function of frequency $\omega = 2\pi f$.

Fluid type	**Flow index** m [-]	**Consistency index** K_m [Pa·s^m]	**Density** ρ_f [kg/m^3]
Water	1	0.001	997
Ketchup	0.3	6.47	1136
Soybean oil	0.51	2.18	930
Ethylene-Glycol	1.29	0.0011	1110

Table 3.3: Rheological properties and densities of water (Newtonian, $K_{m=1} = \mu_0$) [21], Ketchup (shear-thinning) [22], Soybean oil (shear-thinning) [23] and Ethylene-Glycol (shear-thickening) [24].

3.1.7 Stability, convergence and benchmark

In the proposed numerical model the Forward Time Centered Space (FTCS) method is utilised to solve the governing momentum equation, 3.7. It uses discrete step sizes in time and space in order to obtain a physical result. It is important that if small errors occur in the model these errors die out rather than magnify, also known as *numerical stability*. The FTCS method for Newtonian fluids is stable this model if [19]:

$$\frac{\mu_0}{\rho_f} \cdot \frac{\Delta t}{(\Delta y)^2} \leq \frac{1}{2} \tag{3.20}$$

where μ_0 is the dynamic viscosity, ρ_f the density, Δt the step size in time and Δy the step size in space. In case of Power-law fluids it is tempting to state that the stability condition can be defined as:

$$\frac{K_m}{\rho_f} \cdot \frac{\Delta t}{(\Delta y)^{1+m}} \leq \frac{1}{2} \tag{3.21}$$

where m and K_m are the rheological properties of the Power-law liquid. Note that if $m = 1$, the Newtonian stability condition is retrieved since $K_1 = \mu_0$. However, equation 3.21 did not prove to be a strict stability condition since in some Power-law calculations stability was achieved even though the value of equation 3.21 was larger than 1/2. Therefore, for every individual set of step sizes $(\Delta t, \Delta y)$ used to obtain results it is verified that the solution of the velocity profile of Power-law fluids is stable, i.e. errors die out rather than magnify.

On top of stability one wants that if smaller and smaller step sizes are taken, the solution of the system *converges* to a constant value (if known, the theoretical value). For all models that will be used convergence of the velocity profile will be checked and the set of step sizes $(\Delta t, \Delta y)$ with the best characteristics, i.e. not too small because of computation time and not too large because of accuracy, will be used in the numerical experiments. Thus small changes occur in the velocity profile for smaller Δt which eventually vanish.

The step sizes Δy, in the fluid, and Δz, in the waveguide, depend heavily on the rheological properties since in case of a strong shear-thickening fluid the viscous skin depth will be larger and the attenuation will be higher than in shear-thinning cases. Therefore for each fluid a combination of Δy and Δz is chosen such that it matches their physical order of magnitude.

To check if the numerical model that will be used gives an accurate result a benchmark case is investigated. The goal of this benchmark case is to obtain the attenuation coefficient of water, $m = 1$, by using the amplitude measurements created by the numerical model. By making use of the result of equation 2.27 the attenuation coefficient for water can be determined experimentally and its validity can be checked by comparing it with the analytical solution of the attenuation coefficient given by equation 2.25.

In the figures 3.1a and 3.1b the analytical and numerical solutions to the velocity profiles of an ultrasonic shear-wave in water are shown for two different time periods, namely for $t_1 = 1T$ and $t_2 = 16T$ where T is one full period. In table 3.4 the experimentally determined

attenuation coefficients are depicted with their corresponding deviation from the analytical value.

The numerical velocity profile during the first period, $1T$, deviates from the analytical velocity profile whereas the velocity profile of the sixteenth period, $16T$, coincides with the analytical solution. This is due to the fact that during the first period the wave still has to reach steady periodic flow. According to Ai [13] the time it takes before the velocity profile reaching steady flow depends on the flow index m. This results in that the more periods are taken, the more overlap between the numerical solution and the analytical solution and thus more accurate results for the experimentally found attenuation coefficients.

Figure 3.2 shows the deviation between the theoretical and experimentally obtained viscosity as a function of the number of periods taken. Even though a larger number of periods taken makes for a smaller deviation from the theoretical value, the model is limited by computation power. Therefore in this study a standard number of periods taken is: $8T$, as a balance between accuracy and computation time.

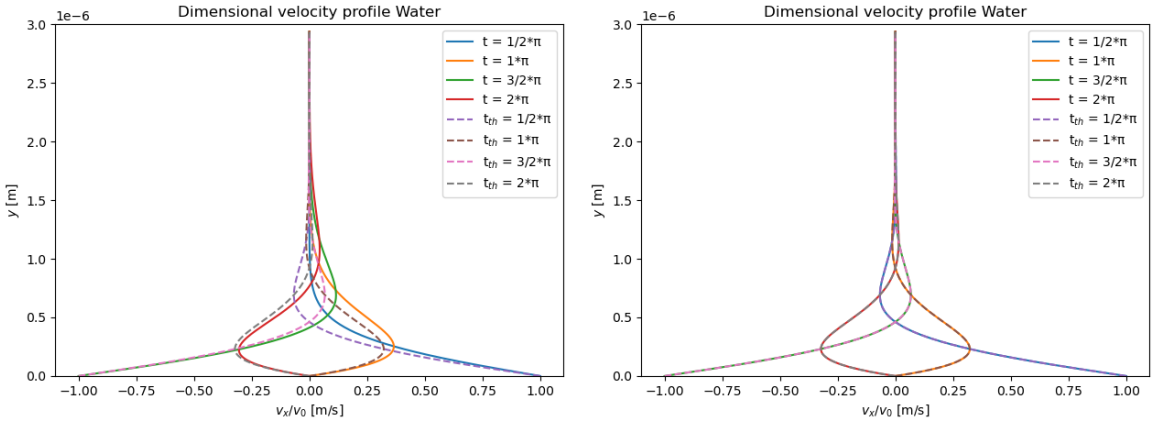

(a) Velocity profiles first period, $1T$.

(b) Velocity profiles sixteenth period, $16T$.

Figure 3.1: Velocity profiles for two time periods of benchmark case (water). The step sizes used: $\Delta t = 9.009 \cdot 10^{-12}$ [s], $\Delta y = 5.875 \cdot 10^{-9}$ [m], $\Delta z = 0.0025$ [m] and used frequency: $f = 3.7$ [MHz]. The dashed lines (- -) are the analytical solutions of the velocity profile whereas the solid line (-) depicts the numerical solutions of the velocity profile.

# of periods	α_{exp} [m^{-1}]	Deviation from theory [%]
$1T$	0.6442	7.17
$16T$	0.6911	0.409

Table 3.4: Benchmark case (water). Obtained attenuation coefficients compared to the theoretical solution to the attenuation coefficient: $\alpha_{th} = 0.6940$ [m^{-1}]. The step sizes used: $\Delta t = 9.009 \cdot 10^{-12}$ [s] and $\Delta y = 5.875 \cdot 10^{-9}$ [m]. Immersion depths $l_{1,2} = n_{l_{1,2}} \cdot \Delta z$ used: $l_1 : n_{l_1} = 100$ and $l_2 : n_{l_2} = 200$ with $\Delta z = 0.0025$ [m]. Frequency used: $f = 3.7$ [MHz].

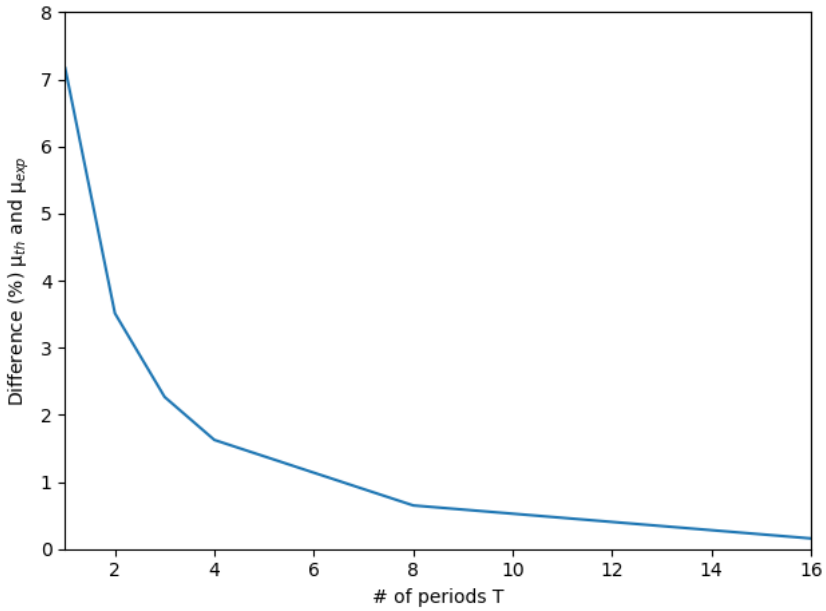

Figure 3.2: Deviation between the theoretical and experimentally obtained viscosity of water as a function of the number of periods taken using the ultrasonic waveguide viscometer model; frequency used: $f = 3.7$ [MHz].

3.2 Methods of retrieving the rheological properties

This section focuses on developing methods to obtain the rheological properties m and K_m of the Power-law fluid ketchup (shear-thinning), soybean oil (shear-thinning) and ethylene-glycol (shear-thickening) using the numerically created amplitude measurements of the numerical viscometer. There are six different methods developed. These methods are numbered with roman numerals for clarity when comparing the results in chapter 4.

Methods I, II, III and IV make use of equations 2.41 and 2.42, which are based on the shear-rate of equation 2.37, as solution to the energy equation 2.10.

Method V uses equations 2.50 and 2.51, which are based on the shear-rate of equation 2.48, as solution to the energy equation 2.10.

Methods VI and VII use equations 2.54 and 2.55, which are based on the shear-rate of equation 2.52, as solution to the energy equation 2.10.

3.2.1 Method I

The idea of this method is that the solution of the energy equation of a Power-law fluid, equation 2.41, can be linearised such that the rheological property K_m can be isolated as constant and the created variable contains all the other parameters such as the flow index m, the immersion depth l and the frequency ω. By varying the immersion depth and frequency separately, two linear fitting methods are proposed: Method I using immersion depth as variable and Method II using frequency as variable.

Method I is proposed by Rohde [11] and investigated by Borstlap [14]. By rewriting the solution to the energy equation 2.41 in a linear form such that it goes through the origin, given in equation 3.24, the flow index m needs to be iterated to find the corresponding K_m. The only physical variable that is changed is the immersion depth l, the frequency $\omega = 2\pi \cdot 3.7$ [MHz] is fixed. The initial velocity amplitude is given by: $B_0 = -\omega \cdot A(0)$. The proposed method is given by the following set of equations:

$$\Delta B^*_\omega(l) \equiv \left(B(\omega, l)^{1-m} - B_0(\omega, 0)^{1-m}\right)^{2/(2-m)} \tag{3.22}$$

$$\Delta l^* \equiv \left(4\frac{P_3(m)}{\rho_s c_s h}|1-m| \cdot (\rho_f \omega)^{m/2} \cdot l\right)^{2/(2-m)} \tag{3.23}$$

$$\Delta B^*_\omega(l) = K_m \cdot \Delta l^* \tag{3.24}$$

To find the values for m and K_m, as described by Borstlap [14], the data set $[\Delta l^*, \Delta B^*_\omega(l)]$ is created by using equations 3.22 and 3.23 and the measured signals $B(\omega, l)$ from the numerical viscometer for each fluid, equation 3.16. These data sets are determined for a range of flow indices m. The range of the m-values used are m_{fit}:[0.1, 0.995] with step size $\Delta m = 0.0045$ for ketchup and soybean oil and m_{fit}:[1.005, 1.9] with step size $\Delta m = 0.0045$ for ethyleneglycol. The created data sets are then fitted to a linear equation $y_{fit} = a \cdot \Delta l^* + b$ using the POLYFIT function of *NumPy* [25]. By minimising the following equation the value for m and K_m can found:

$$\epsilon(m_{fit}) = \sum_{k=1}^{N_l} \sqrt{(y_{fit}(l_k, mfit) - \Delta B^*_\omega(l_k, m_{fit}))^2} \tag{3.25}$$

with immersion depth: $l_k = k \cdot \Delta z$, where k is the number of steps with maximum $N_l = 200$. If $\epsilon(m_{fit}) \to 0$ the corresponding flow index m_{fit} is the flow index of the used Power-law fluid and the value of (a) is the same as the consistency index K_m of the used Power-law fluid.

3.2.2 Method II

Method II is based on method I which linearises the energy equation of a Power-law fluid, equation 2.41. However, in this method the frequency ω is used as variable and not the immersion depth l. The set of equations used in this method come from the equations of Borstlap [14], equations 3.22, 3.23 and 3.24. To clarify that the immersion depth is fixed

in this method l is put as a subscript in $\Delta B_l^*(\omega)$. The fixed immersion depth is given by: $l = n_l \cdot \Delta z$, where n_l is the number of step taken and Δz is the step size per fluid. The initial velocity amplitude is given by: $B_0 = -\omega \cdot A(0)$. By fitting the created data set $[\Delta l^*, \Delta B_l^*(\omega)]$ to a linear function, m and K_m can be found.

$$\Delta B_l^*(\omega) \equiv \left(B(\omega, l)^{1-m} - B_0(\omega, 0)^{1-m}\right)^{2/(2-m)} \tag{3.26}$$

$$\Delta l^* \equiv \left(4\frac{P_3(m)}{\rho_s c_s h}|1-m| \cdot (\rho_f \omega)^{m/2} \cdot l\right)^{2/(2-m)} \tag{3.27}$$

$$\Delta B_l^*(\omega) = K_m \cdot \Delta l^* \tag{3.28}$$

The measured data sets $[\omega, B(\omega, l)]$ per fluid, calculated using equation 3.16, are used to find expression of Δl^* and $\Delta B_l^*(\omega)$, determined by equations 3.26 and 3.27, and can be written as linear equation 3.28. These data sets are determined for a range of flow indices m. The range of the m-values used are m_{fit}:[0.1, 0.995] with step size $\Delta m = 0.0045$ for ketchup and soybean oil and m_{fit}:[1.005, 1.9] with step size $\Delta m = 0.0045$ for ethylene-glycol. The created data sets are then fitted to a linear equation $y_{fit} = a \cdot \Delta l^* + b$ using the POLYFIT function of *NumPy* [25]. By minimising the following equation the value for m and K_m can found:

$$\epsilon(m_{fit}) = \sum_{\omega_n} \sqrt{(y_{fit}(\omega_n, mfit) - \Delta B_l^*(\omega_n, m_{fit}))^2} \tag{3.29}$$

The range of frequencies that will be used is ω_n:[3.3-4.3] [MHz] with step sizes of 0.1 [MHz]. If $\epsilon(m_{fit}) \to 0$ the corresponding flow index m_{fit} is the flow index of the used Power-law fluid and the value of (a) found by the linear fit is equal to the consistency index K_m of the used Power-law fluid.

3.2.3 Method III

The methods I and II from sections 3.2.1 and 3.2.2 need a solution to the initial velocity amplitude at zero immersion depth $B_0(\omega)$ to be able to work. This initial velocity amplitude can also be seen as the energy transfer from the transducer to the waveguide, but since this energy transfer is practically not ideal and frequency dependent, it is not known experimentally. Method III and IV are developed to find a way of eliminating the initial velocity amplitude $B_0(\omega)$ and retrieving the rheological properties m and K_m subsequently, making these methods experimentally possible. The difference between these methods is due to the usage of two different conditions on $B_0(\omega)$ in order to eliminate this term. Method III is discussed first.

Method III makes use of equations 2.41 and 2.42, which are based on the shear-rate of equation 2.37, as solution to the energy equation 2.10. The two physical variables that can be controlled experimentally and appear in the solution of the energy equation are the immersion depth l and the frequency ω. By using two different immersion depths, l_1 and l_2, and two different frequencies, ω_1 and ω_2, four sets of solutions to equation 2.41 can be found:

$$\omega_1, l_1 : B(\omega_1, l_1)^{1-m} - B_0(\omega_1, l_1)^{1-m} = 2 \cdot l_1 \cdot (1-m) \cdot \alpha_m(\omega_1) \tag{3.30}$$
$$\omega_1, l_2 : B(\omega_1, l_2)^{1-m} - B_0(\omega_1, l_2)^{1-m} = 2 \cdot l_2 \cdot (1-m) \cdot \alpha_m(\omega_1) \tag{3.31}$$
$$\omega_2, l_1 : B(\omega_2, l_1)^{1-m} - B_0(\omega_2, l_1)^{1-m} = 2 \cdot l_1 \cdot (1-m) \cdot \alpha_m(\omega_2) \tag{3.32}$$
$$\omega_2, l_2 : B(\omega_2, l_2)^{1-m} - B_0(\omega_2, l_2)^{1-m} = 2 \cdot l_2 \cdot (1-m) \cdot \alpha_m(\omega_2) \tag{3.33}$$

As can be seen four different velocity amplitudes $B(\omega, l)$ are produced, but also four initial velocity amplitudes. Although the initial amplitude $B_0(\omega)$ can differ per frequency it is the same for fixed frequency and different immersion depths since $B_0(\omega) = -\omega \cdot A(0)$, leading to:

$$B_0(\omega_1, l_1) = B_0(\omega_1, l_2) = B_0(\omega_1) \quad \text{and} \quad B_0(\omega_2, l_1) = B_0(\omega_2, l_2) = B_0(\omega_2) \tag{3.34}$$

By using the result of equation 3.34 and taking the difference between equations 3.30 and 3.31 and between equations 3.32 and 3.33, these unknown initial velocity amplitude terms drop out. What remains are two equations with two unknowns, namely the flow index m and the consistency index K_m which is hidden in α_m (equation 2.42).

$$B(\omega_1, l_1)^{1-m} - B(\omega_1, l_2)^{1-m} = 2 \cdot (1-m) \cdot \alpha_m(\omega_1) \cdot (l_1 - l_2) \tag{3.35}$$
$$B(\omega_2, l_1)^{1-m} - B(\omega_2, l_2)^{1-m} = 2 \cdot (1-m) \cdot \alpha_m(\omega_2) \cdot (l_1 - l_2) \tag{3.36}$$

The next step is to create two expressions to determine the rheological properties m and K_m separately. To do so, equation 3.35 is divided by equation 3.36. Since the only difference between the $\alpha_m(\omega)$'s are the frequency terms, see equation 2.42, what remains is:

$$\frac{B(\omega_1, l_1)^{1-m} - B(\omega_1, l_2)^{1-m}}{B(\omega_2, l_1)^{1-m} - B(\omega_2, l_2)^{1-m}} = \left(\frac{\omega_1}{\omega_2}\right)^{m/2} \tag{3.37}$$

This equation does not contain K_m as it has been divided out. Therefore, equation 3.37 will be used to determine the flow index m. This is done by using the measured velocity amplitudes of the fluids and the corresponding two immersion depths l_1, l_2 and frequencies ω_1, ω_2. The immersion depths and frequencies which are used in the calculations of m per fluid are given in the corresponding result section. The flow index m is found using the *fsolve*-function from *NumPy* [25].
In order to find an expression to calculate the consistency index K_m, equation 3.35 (or 3.36 can also be used) is rewritten such that the following expression for K_m is obtained:

$$K_m = \left[-\frac{B(\omega_1, l_1)^{1-m} - B(\omega_1, l_2)^{1-m}}{4 \cdot |1-m| \cdot (l_1 - l_2) \cdot P_3(m) \cdot (\rho_f \omega_1)^{m/2}} \cdot \rho_s c_s h \right]^{2/(2-m)} \tag{3.38}$$

This equation is used to find the consistency index K_m. This is done by using the measured velocity amplitudes of the fluids and the corresponding two immersion depths l_1, l_2 and frequencies ω_1, ω_2. Furthermore, the value for the flow index m found by equation 3.37 and the constant from table 3.2 are used in the calculation of K_m.

3.2.4 Method IV

This method makes use of equations 2.41 and 2.42, which are based on the shear-rate of equation 2.37, as solution to the energy equation 2.10. This method is developed to find a way of eliminating the initial velocity amplitude $B_0(\omega)$ and retrieving the rheological properties m and K_m subsequently, same as method III. The difference between method III and IV comes from a different condition on the experimentally unknown initial velocity amplitude $B_0(\omega)$.

As stated before, the initial velocity amplitude from the transducer to the waveguide is defined as: $B_0(\omega) = -\omega \cdot A(0)$. This implies that the initial velocity amplitude terms for different frequencies ω_1, ω_2 at a fixed immersion depths l_1, l_2 are equal if:

$$\frac{B_0(\omega_1, l_1)}{\omega_1} = \frac{B_0(\omega_2, l_1)}{\omega_2} \quad \text{and} \quad \frac{B_0(\omega_1, l_2)}{\omega_1} = \frac{B_0(\omega_2, l_2)}{\omega_2} \tag{3.39}$$

Consider again the equations 3.30, 3.31, 3.32, 3.33. In order to remove the unknown $B_0(\omega)$'s by using the result in equation 3.39, these four equation need to be divided by their corresponding frequency ($\omega_{1,2}^{1-m}$) in the following way:

$$\omega_1, l_1 : \frac{B(\omega_1, l_1)^{1-m}}{\omega_1^{1-m}} - \frac{B_0(\omega_1, l_1)^{1-m}}{\omega_1^{1-m}} = 2 \cdot l_1 \cdot (1-m) \cdot \frac{\alpha_m(\omega_1)}{\omega_1^{1-m}} \tag{3.40}$$

$$\omega_1, l_2 : \frac{B(\omega_1, l_2)^{1-m}}{\omega_1^{1-m}} - \frac{B_0(\omega_1, l_2)^{1-m}}{\omega_1^{1-m}} = 2 \cdot l_2 \cdot (1-m) \cdot \frac{\alpha_m(\omega_1)}{\omega_1^{1-m}} \tag{3.41}$$

$$\omega_2, l_1 : \frac{B(\omega_2, l_1)^{1-m}}{\omega_2^{1-m}} - \frac{B_0(\omega_2, l_1)^{1-m}}{\omega_2^{1-m}} = 2 \cdot l_1 \cdot (1-m) \cdot \frac{\alpha_m(\omega_2)}{\omega_2^{1-m}} \tag{3.42}$$

$$\omega_2, l_2 : \frac{B(\omega_2, l_2)^{1-m}}{\omega_2^{1-m}} - \frac{B_0(\omega_2, l_2)^{1-m}}{\omega_2^{1-m}} = 2 \cdot l_2 \cdot (1-m) \cdot \frac{\alpha_m(\omega_2)}{\omega_2^{1-m}} \tag{3.43}$$

By using the result of equation 3.39 and taking the difference between equations 3.40 and 3.42 and between equations 3.41 and 3.43, the unknown initial velocity amplitude terms drop out. What remains are two equations with two unknowns, namely the flow index m and the consistency index K_m which is hidden in $\alpha_m(\omega)$ (equation 2.42).

$$\left[\frac{B(\omega_1, l_1)}{\omega_1}\right]^{1-m} - \left[\frac{B(\omega_2, l_1)}{\omega_2}\right]^{1-m} = 2 \cdot l_1 \cdot (1-m) \cdot \left[\frac{\alpha_m(\omega_1)}{\omega_1^{1-m}} - \frac{\alpha_m(\omega_2)}{\omega_2^{1-m}}\right] \tag{3.44}$$

$$\left[\frac{B(\omega_1, l_2)}{\omega_1}\right]^{1-m} - \left[\frac{B(\omega_2, l_2)}{\omega_2}\right]^{1-m} = 2 \cdot l_2 \cdot (1-m) \cdot \left[\frac{\alpha_m(\omega_1)}{\omega_1^{1-m}} - \frac{\alpha_m(\omega_2)}{\omega_2^{1-m}}\right] \tag{3.45}$$

Similar to method III, the next step is to create two separate expressions to determine the rheological properties m and K_m. The expression to find the flow index m equation 3.44 is divided by equation 3.45. Since the only difference between the RHS's of the equations is the immersion depth, what remains is:

$$\frac{\left[\frac{B(\omega_1,l_1)}{\omega_1}\right]^{1-m} - \left[\frac{B(\omega_2,l_1)}{\omega_2}\right]^{1-m}}{\left[\frac{B(\omega_1,l_2)}{\omega_1}\right]^{1-m} - \left[\frac{B(\omega_2,l_2)}{\omega_2}\right]^{1-m}} = \frac{l_1}{l_2} \tag{3.46}$$

The only unknown of this equation is the flow index m and can therefore be found. This is done by using the measured velocity amplitudes of the fluids and the corresponding two immersion depths l_1, l_2 and frequencies ω_1, ω_2. The immersion depths and frequencies which are used in the calculations of m per fluid are given in the corresponding result section. The flow index m is found using the *fsolve*-function from *NumPy* [25].
To find the expression to calculate the consistency index K_m, equation 3.44 (or 3.45) is rewritten such that:

$$K_m = \left[\frac{\frac{B(\omega_1,l_1)^{1-m}}{\omega_1^{1-m}} - \frac{B(\omega_2,l_1)^{1-m}}{\omega_2^{1-m}}}{\omega_1^{m/2} - \omega_2^{m/2}} \cdot \frac{\rho_s c_s h}{4 \cdot |1-m| \cdot l_1 \cdot P_3(m) \cdot \rho_f^{m/2}}\right]^{2/2-m} \tag{3.47}$$

This equation is used to find the consistency index K_m. This is done by using the measured velocity amplitudes of the fluids and the corresponding two immersion depths l_1, l_2 and frequencies ω_1, ω_2. Furthermore, the value for the flow index m found by equation 3.46, the fluid's density ρ_f and the constant from table 3.2 are used in the calculation of K_m.

3.2.5 Method V

Method V uses equations 2.50 and 2.51, which are based on the shear-rate of equation 2.48, as solution to the energy equation 2.10. Notice that the shear-rate used in this method differs from the shear-rate, equation 2.37, used in methods I, II, III and IV. However, the approach to find the solutions of the flow index m and the consistency index K_m in method V by eliminating the initial velocity amplitude $B_0(\omega)$ is similar to the approach used in method IV, section 3.2.4.

The immersion depth l and the frequency ω are the two variables that can be controlled experimentally and appear in the solution to the energy equation 2.50. Using two different immersion depths, l_1 and l_2, and two different frequencies, ω_1 and ω_2, four sets of solutions to equation 2.50 can be found. By dividing these four equation by a specific power of the corresponding frequency ($\omega_{1,2}^{1-m}$), the four obtained equations are:

$$\omega_1, l_1 : \frac{B(\omega_1,l_1)^{1-m}}{\omega_1^{1-m}} - \frac{B_0(\omega_1,l_1)^{1-m}}{\omega_1^{1-m}} = 2 \cdot l_1 \cdot (1-m) \cdot \frac{\alpha_s(\omega_1)}{\omega_1^{1-m}} \tag{3.48}$$

$$\omega_1, l_2 : \frac{B(\omega_1,l_2)^{1-m}}{\omega_1^{1-m}} - \frac{B_0(\omega_1,l_2)^{1-m}}{\omega_1^{1-m}} = 2 \cdot l_2 \cdot (1-m) \cdot \frac{\alpha_s(\omega_1)}{\omega_1^{1-m}} \tag{3.49}$$

$$\omega_2, l_1 : \frac{B(\omega_2,l_1)^{1-m}}{\omega_2^{1-m}} - \frac{B_0(\omega_2,l_1)^{1-m}}{\omega_2^{1-m}} = 2 \cdot l_1 \cdot (1-m) \cdot \frac{\alpha_s(\omega_2)}{\omega_2^{1-m}} \tag{3.50}$$

$$\omega_2, l_2 : \frac{B(\omega_2,l_2)^{1-m}}{\omega_2^{1-m}} - \frac{B_0(\omega_2,l_2)^{1-m}}{\omega_2^{1-m}} = 2 \cdot l_2 \cdot (1-m) \cdot \frac{\alpha_s(\omega_2)}{\omega_2^{1-m}} \tag{3.51}$$

By using the result of equation 3.39 and taking the difference between equations 3.48 and 3.50 and between equations 3.49 and 3.51, the unknown initial velocity amplitude terms dropout. What remains are two equations with two unknowns, namely the flow index m and the consistency index Km which is hidden in $\alpha_s(\omega)$ (equation 2.51):

$$\left[\frac{B(\omega_1, l_1)}{\omega_1}\right]^{1-m} - \left[\frac{B(\omega_2, l_1)}{\omega_2}\right]^{1-m} = 2 \cdot l_1 \cdot (1-m) \cdot \left[\frac{\alpha_s(\omega_1)}{\omega_1^{1-m}} - \frac{\alpha_s(\omega_2)}{\omega_2^{1-m}}\right] \tag{3.52}$$

$$\left[\frac{B(\omega_1, l_2)}{\omega_1}\right]^{1-m} - \left[\frac{B(\omega_2, l_2)}{\omega_2}\right]^{1-m} = 2 \cdot l_2 \cdot (1-m) \cdot \left[\frac{\alpha_s(\omega_1)}{\omega_1^{1-m}} - \frac{\alpha_s(\omega_2)}{\omega_2^{1-m}}\right] \tag{3.53}$$

To create two separate expressions to determine the rheological properties m and K_m equation 3.52 is divided by equation 3.53. Since the only difference between the RHS's of these equations is the difference in immersion depth, what remains is:

$$\frac{\left[\frac{B(\omega_1,l_1)}{\omega_1}\right]^{1-m} - \left[\frac{B(\omega_2,l_1)}{\omega_2}\right]^{1-m}}{\left[\frac{B(\omega_1,l_2)}{\omega_1}\right]^{1-m} - \left[\frac{B(\omega_2,l_2)}{\omega_2}\right]^{1-m}} = \frac{l_1}{l_2} \tag{3.54}$$

Notice that this equation is equal to equation 3.46 in method IV. Equation 3.54 is used to calculated the flow index m. This is done by using the measured velocity amplitudes of the fluids and the corresponding two immersion depths l_1, l_2 and frequencies ω_1, ω_2. The immersion depths and frequencies which are used in the calculations of m per fluid are given in the corresponding result section. The flow index m is found using the *fsolve*-function from *NumPy* [25].

To find the expression to calculate the consistency index K_m, equation 3.52 (or 3.53) is rewritten such that:

$$K_m = \left[\frac{\frac{B(\omega_1,l_1)^{1-m}}{\omega_1^{1-m}} - \frac{B(\omega_2,l_1)^{1-m}}{\omega_2^{1-m}}}{\left(\frac{\omega_1^{m^2+m-1}}{B_0^{m^2-m}(\omega_1)}\right)^{\frac{1}{m+1}} - \left(\frac{\omega_2^{m^2+m-1}}{B_0^{m^2-m}(\omega_2)}\right)^{\frac{1}{m+1}}} \cdot \frac{\rho_s c_s h}{4 \cdot |1-m| \cdot l_1 \cdot P_3(m) \cdot \rho_f^{\frac{m}{m+1}}}\right]^{m+1} \tag{3.55}$$

This equation is used to calculated the consistency index K_m. This is done by using the measured velocity amplitudes of the fluids and the corresponding two immersion depths l_1, l_2 and frequencies ω_1, ω_2. Furthermore, the value for the flow index m found by equation 3.54, the fluid's density ρ_f and the constant from table 3.2 are used in the calculation of K_m.

However, in equation 3.55 terms of the initial velocity amplitude are still present, making this method undesirable experimentally. If $B_0(\omega)$ would be known, this method would be usable experimentally. Numerically, the values are calculated by using $B_0(\omega) = -\omega \cdot A(0)$.

3.2.6 Method VI

This method uses equations 2.54 and 2.55 as solution to the energy equation 2.10, which are based on the shear-rate of equation 2.52. Notice that the shear-rate used in this method differs from the shear-rates used in methods I, II, III, IV and V, which use equation 2.37 and equation 2.48 for the shear-rate respectively. The approach to find the solutions of the flow index m and the consistency index K_m in method VI by eliminating the initial velocity amplitude $B_0(\omega)$ is similar to the approach used in method IV, section 3.2.4.

The immersion depth l and the frequency ω are the two variables that can be controlled experimentally and appear in the solution to the energy equation 2.54. Using two different immersion depths, l_1 and l_2, and two different frequencies, ω_1 and ω_2, four sets of solutions to equation 2.54 can be found. By dividing these four equation by a specific power of the corresponding frequency ($\omega_{1,2}^{1-m}$), the four obtained equations are:

$$\omega_1, l_1 : \frac{B(\omega_1, l_1)^{1-m}}{\omega_1^{1-m}} - \frac{B_0(\omega_1, l_1)^{1-m}}{\omega_1^{1-m}} = 2 \cdot l_1 \cdot (1-m) \cdot \frac{\alpha_r(\omega_1)}{\omega_1^{1-m}} \tag{3.56}$$

$$\omega_1, l_2 : \frac{B(\omega_1, l_2)^{1-m}}{\omega_1^{1-m}} - \frac{B_0(\omega_1, l_2)^{1-m}}{\omega_1^{1-m}} = 2 \cdot l_2 \cdot (1-m) \cdot \frac{\alpha_r(\omega_1)}{\omega_1^{1-m}} \tag{3.57}$$

$$\omega_2, l_1 : \frac{B(\omega_2, l_1)^{1-m}}{\omega_2^{1-m}} - \frac{B_0(\omega_2, l_1)^{1-m}}{\omega_2^{1-m}} = 2 \cdot l_1 \cdot (1-m) \cdot \frac{\alpha_r(\omega_2)}{\omega_2^{1-m}} \tag{3.58}$$

$$\omega_2, l_2 : \frac{B(\omega_2, l_2)^{1-m}}{\omega_2^{1-m}} - \frac{B_0(\omega_2, l_2)^{1-m}}{\omega_2^{1-m}} = 2 \cdot l_2 \cdot (1-m) \cdot \frac{\alpha_r(\omega_2)}{\omega_2^{1-m}} \tag{3.59}$$

By using the result of equation 3.39 and taking the difference between equations 3.56 and 3.58 and between equations 3.57 and 3.59, the unknown initial velocity amplitude terms dropout. What remains are two equations with two unknowns, namely the flow index m and the consistency index Km which is hidden in $\alpha_r(\omega)$ (equation 2.55):

$$\left[\frac{B(\omega_1, l_1)}{\omega_1}\right]^{1-m} - \left[\frac{B(\omega_2, l_1)}{\omega_2}\right]^{1-m} = 2 \cdot l_1 \cdot (1-m) \cdot \left[\frac{\alpha_r(\omega_1)}{\omega_1^{1-m}} - \frac{\alpha_r(\omega_2)}{\omega_2^{1-m}}\right] \tag{3.60}$$

$$\left[\frac{B(\omega_1, l_2)}{\omega_1}\right]^{1-m} - \left[\frac{B(\omega_2, l_2)}{\omega_2}\right]^{1-m} = 2 \cdot l_2 \cdot (1-m) \cdot \left[\frac{\alpha_r(\omega_1)}{\omega_1^{1-m}} - \frac{\alpha_r(\omega_2)}{\omega_2^{1-m}}\right] \tag{3.61}$$

In order to create two separate expressions to determine the rheological properties m and K_m equation 3.60 is divided by equation 3.61. Since the only difference between the RHS's of these equations is the difference in immersion depth, what remains is:

$$\frac{\left[\frac{B(\omega_1, l_1)}{\omega_1}\right]^{1-m} - \left[\frac{B(\omega_2, l_1)}{\omega_2}\right]^{1-m}}{\left[\frac{B(\omega_1, l_2)}{\omega_1}\right]^{1-m} - \left[\frac{B(\omega_2, l_2)}{\omega_2}\right]^{1-m}} = \frac{l_1}{l_2} \tag{3.62}$$

Notice that this equation is equal to equation 3.46 in method IV and equation 3.54 in method V. Equation 3.62 is used to calculated the flow index m. This is done by using the measured velocity amplitudes of the fluids and the corresponding two immersion depths l_1, l_2 and frequencies ω_1, ω_2. The immersion depths and frequencies which are used in the calculations of m per fluid are given in the corresponding result section. The flow index m is found using the *fsolve*-function from *NumPy* [25].

To find the expression to calculate the consistency index K_m, equation 3.60 (or 3.61) is rewritten such that:

$$K_m = \rho_s c_s h \cdot \frac{\frac{B(\omega_1,l_1)^{1-m}}{\omega_1^{1-m}} - \frac{B(\omega_2,l_1)^{1-m}}{\omega_2^{1-m}}}{4 \cdot |1-m| \cdot l_1 \cdot P_3(m) \cdot \rho_f^{m/2}} \cdot \left[\frac{\omega_1^{\frac{3m-2}{2}}}{[\mu_{app}(\omega_1)]^{m/2}} - \frac{\omega_2^{\frac{3m-2}{2}}}{[\mu_{app}(\omega_2)]^{m/2}} \right]^{-1} \tag{3.63}$$

This equation is used to calculate the consistency index K_m by using measured velocity amplitudes of the fluids and the corresponding two immersion depths l_1, l_2 and frequencies ω_1, ω_2. Furthermore, the value for the flow index m found by equation 3.62, the fluid's density ρ_f and the constant from table 3.2 are used in the calculation of K_m. Lastly, two solutions to the apparent viscosity term $\mu_{app}(\omega)$ need to be obtained to find K_m using equation 3.63. Two different approaches to find these values are used: Approach A uses a *numerical* solution and Approach B uses a *analytical* solution.

Approach A

By using the solution to shear-rate on the boundary ($i = 0$) of equation 3.12 in combination with the theoretical expression of the apparent viscosity in Power-law fluids, equation 2.14, the numerical solution of the apparent viscosity is obtained:

$$\mu_{app}(\omega) = K_m \cdot |\dot{\gamma}_{i=0}|^{m-1} \tag{3.64}$$

To obtain a single value for $\mu_{app}(\omega)$, the average value of equation 3.64 is taken since $\dot{\gamma}_{i=0}$ is a function of time, equation 3.12. The rheological properties per fluid used in calculation of $\dot{\gamma}_{i=0}$ and 3.64 are given in table 3.3.

Since the solution of $\mu_{app}(\omega)$ is calculated numerically, this approach cannot be used experimentally for the calculation of the consistency index K_m in equation 3.63. Therefore, in order to find K_m using equation 3.63 experimentally, Approach B is proposed.

Approach B

In this approach an analytical expression of the apparent viscosity $\mu_{app}(\omega)$ is proposed to find the consistency index K_m in equation 3.63 experimentally. By using theoretical expression 2.14 of the apparent viscosity, the following equation is obtained:

$$\mu_{app}(\omega) \sim K_m \cdot \omega^{m-1} \tag{3.65}$$

where the assumption has been made that $\dot{\gamma}_{PL} \sim \omega$, which most certainly needs revision in follow-up studies. This proposed apparent viscosity has the correct units [Pa·s], contains the rheological properties m, K_m and frequency term ω. Substituting expression 3.65 of the apparent viscosity in equation 3.63 results in a new expression to find the consistency index K_m. Rewriting yields the following equation:

$$K_m = \left[\rho_s c_s h \cdot \frac{\frac{B(\omega_1,l_1)^{1-m}}{\omega_1^{1-m}} - \frac{B(\omega_2,l_1)^{1-m}}{\omega_2^{1-m}}}{4 \cdot |1-m| \cdot l_1 \cdot P_3(m) \cdot \rho_f^{m/2}} \cdot \left[\frac{\omega_1^{\frac{-m^2+2m}{2}}}{\omega_1^{1-m}} - \frac{\omega_2^{\frac{-m^2+2m}{2}}}{\omega_2^{1-m}} \right]^{-1} \right]^{\frac{2}{2-m}} \tag{3.66}$$

This equation is used to calculate the consistency index K_m with Approach B by using the measured velocity amplitudes of the fluids and the corresponding two immersion depths l_1, l_2 and frequencies ω_1, ω_2. The value for the flow index m calculated by equation 3.62, the fluid's density ρ_f and the constant from table 3.2 are used in this calculation of K_m.

Chapter 4

Results and discussion

This chapter displays and discusses the obtained results of the proposed methods I, II, III, IV, V and VI by using the numerical viscometer described in chapter 3. All the parameters necessary in the determination of the results are given in that chapter, otherwise it will be mentioned accordingly. The goal of these experimental methods is to retrieve the rheological properties of known Power-law fluids accurately using the amplitude measurements of the ultrasonic waveguide viscometer.

First the solutions to the dimensional velocity profiles and attenuation of the shear-wave amplitudes are shown for fluids ketchup (shear-thinning), soybean oil (shear-thinning) and ethylene-glycol (shear-thickening) by using equations 3.10 and 3.16. Subsequently, the dimensionless velocity profiles and dimensionless shear-rates are shown.

4.1 Velocity profile and amplitude attenuation

The dimensional velocity profiles of the used fluids and their amplitude attenuation of the shear-wave with a frequency of $f = 3.7$ [MHz] in the waveguide are displayed in this section. The dimensional velocity profile plots for ketchup, soybean oil and ethylene-glycol are shown in the figures 4.1a, 4.2a and 4.3a. It is important to note the difference in the order of magnitude of the y-axes between the three fluids. It shows that the penetration depth (viscous skin depth) of the shear-wave in ethylene-glycol is larger than the shear-wave in ketchup or soybean oil. The shape of the velocity profiles also differs for each of the fluids.

The figures 4.1b, 4.2b and 4.3b show the amplitude attenuation of the shear-wave in the waveguide as a function of z, the travelled distance of the wave in the immersed waveguide. The plots show a large difference in length travelled until the velocity amplitude reaches zero value. This difference in total travelled length until it vanishes relates to the amount of attenuation of the shear-wave in the waveguide due to the rheological properties of the fluid in which it is immersed. The more viscous a fluid, the more energy is dissipated in that fluid and thus the higher the attenuation of the shear-wave in the waveguide. Therefore, the steeper attenuation of the velocity amplitude of ethylene-glycol in comparison with ketchup was expected.

Since the actual waveguide has a length of about 20 [cm] the attenuation distance of ethylene-glycol is too short to give measurable amplitude attenuation in the physical setup. For ketchup the attenuation distance seems too large for the signal in the physical setup to be measurably attenuated. It would be interesting to verify the experimental possibility of measurable amplitude differences for fluids like ketchup and ethylene-glycol to check if the methods described in chapter 3 are feasible experimentally.

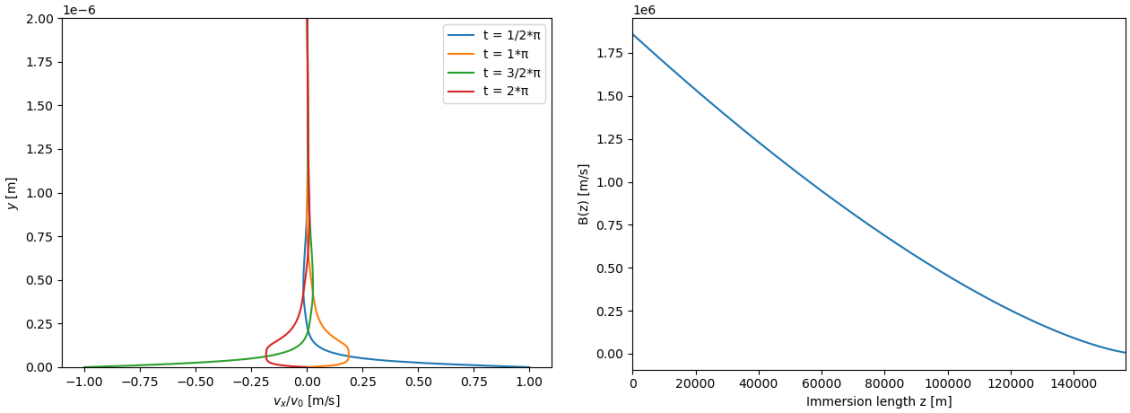

(a) Velocity profile

(b) Amplitude attenuation

Figure 4.1: **Ketchup** ($m = 0.3$, $K_m = 6.47$ [Pa·s^m]): Developed dimensional velocity profile and amplitude attenuation plot. The step sizes used are: $\Delta t = 9.009 \cdot 10^{-12}$ [s], $\Delta y = 4.677 \cdot 10^{-9}$ [m], $\Delta z = 158.5$ [m] and used frequency: $f = 3.7$ [MHz].

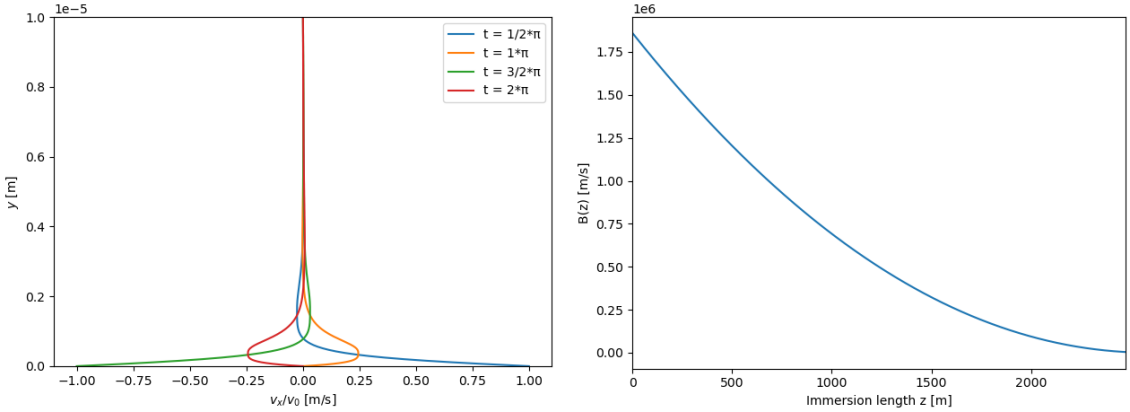

(a) Velocity amplitude

(b) Amplitude attenuation

Figure 4.2: **Soybean oil** ($m = 0.51$, $K_m = 2.18$ [Pa·s^m]): Developed dimensional velocity profile and amplitude attenuation plot. The step sizes used are: $\Delta t = 9.009 \cdot 10^{-12}$ [s], $\Delta y = 2.226 \cdot 10^{-8}$ [m], $\Delta z = 2.507$ [m] and used frequency: $f = 3.7$ [MHz].

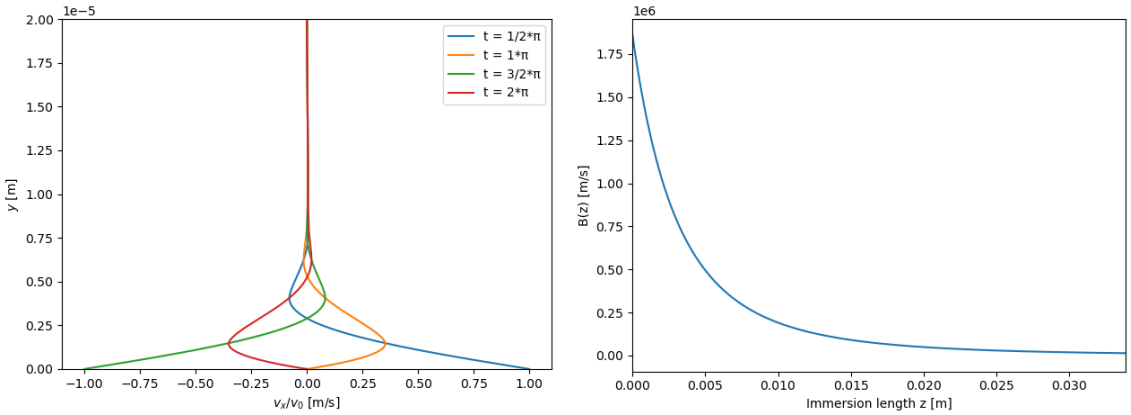

(a) Velocity profile

(b) Amplitude attenuation

Figure 4.3: **Ethylene-Glycol** ($m = 1.29$, $K_m = 0.0011$ [Pa·s^m]): Developed dimensional velocity profile and amplitude attenuation plot. The step sizes used are: $\Delta t = 9.009 \cdot 10^{-12}$ [s], $\Delta y = 6.831 \cdot 10^{-8}$ [m], $\Delta z = 3.433 \cdot 10^{-5}$ [m] and used frequency: $f = 3.7$ [MHz].

4.2 Velocity profiles and shear-rates constant κ condition

In this section results are shown of dimensionless velocity profiles, dimensionless shear-rates and dimensional shear-rates using the constant κ condition of equation 2.44. These results are obtained by using equations 3.17, 3.18 and 3.12 respectively. Using the reference parameters of table 3.1, the dimensionless constant κ, equation 2.34, can be calculated.

4.2.1 Dimensionless velocity profile

Using the following combinations of rheological properties two different values for κ are calculated, namely: $m = 0.5$ with $K_m = 2.5 \cdot 10^3$ [Pa·s^m] result in $\kappa = 0.83$, and $m = 1.5$ with $K_m = 4.1 \cdot 10^{-10}$ [Pa·s^m] results in $\kappa = 1.23$. The figure 4.4a shows the dimensionless velocity profile for $\kappa = 0.83$ and 4.4b shows the dimensionless velocity profile for $\kappa = 1.23$. The dotted lines in both figures represent the dimensionless result of the velocity profiles for $m = 0.5$ and $m = 1.5$ shown in figure 2.4 from Ai & Vafai.

In section 2.6.3 the idea is proposed that the dimensionless shear-rates on the boundary for different combinations of rheological properties are equal if their corresponding κ's are equal. This idea was deduced from the result of figure 2.4 from Ai & Vafai [13] and expressed in equation 2.43. In the next section the dimensionless velocity profiles for combinations of rheological properties (m, K_m) and constant κ are shown.

4.2.2 Dimensionless velocity profiles and shear-rates constant κ

In this section dimensionless velocity profile plots are shown using a constant value for κ at four different time intervals created by two different sets of rheological properties (m, K_m). The used κ's are $\kappa = 0.83$ and $\kappa = 1.23$ which are also used in figure 4.4. In the figures 4.5 and 4.6 the dimensionless velocity profiles are shown for these values of κ. The two sets of

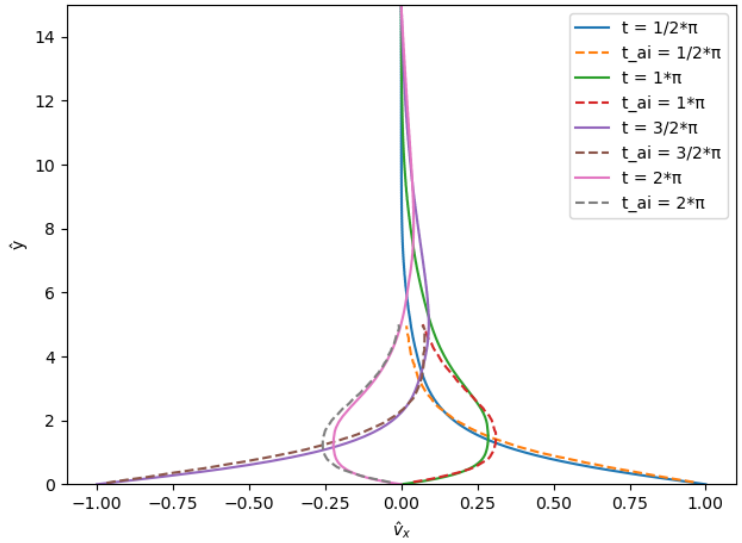

(a) $m = 0.5$, $K_m = 2.5 \cdot 10^3$ [Pa·s^m], $\kappa = 0.83$

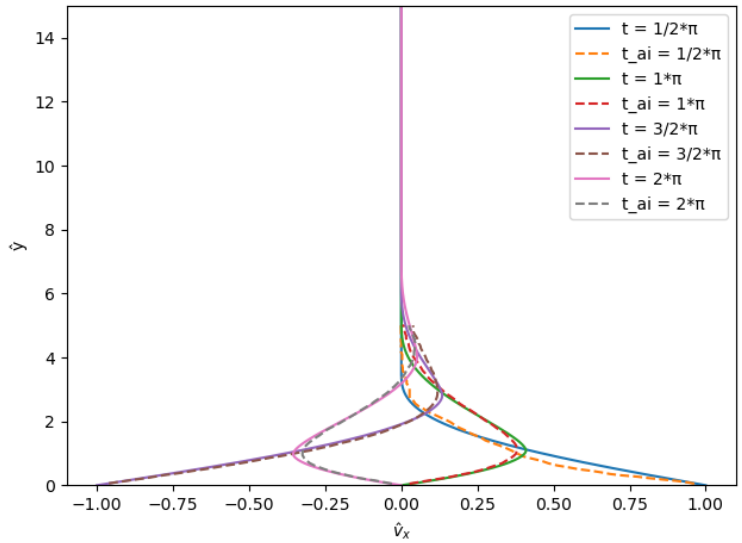

(b) $m = 1.5$, $K_m = 4.1 \cdot 10^{-10}$ [Pa·s^m], $\kappa = 1.23$

Figure 4.4: Dimensionless velocity profiles for $\kappa = 0.83$ and $\kappa = 1.23$ at four time intervals (solid lines) compared to dimensionless result of the velocity profiles for $m = 0.5$ and $m = 1.5$ (dashed lines) shown in figure 2.4 [13]. The reference constants used to determine κ are given in table 3.1. The non-dimensional step size are: $\Delta\hat{t} = 2.094 \cdot 10^{-4}$ and $\Delta\hat{y} = 3.000 \cdot 10^{-2}$.

rheological properties (m, K_m) used to calculated the constant κ are given in the captions of the figures. The flow profile of the velocity needs time to develop, about one full period, which causes that the developing velocity profiles are different from the developed velocity profiles. Therefore, the result are shown for both developing flow and developed flow. The dimensionless step sizes $\Delta\hat{t}$ and $\Delta\hat{y}$ are the same as the step sizes used in figure 4.4.

In figure 4.5a and 4.5b, for developing flow and fully developed flow, it can be seen that the dimensionless velocity profiles near the boundary almost overlap for different flow indices, for constant $\kappa = 0.83$. This is a promising result for finding dimensionless equal shear-rates on the boundary. The same result is obtain if constant $\kappa = 1.23$ is used, see figure 4.6a and 4.6b.

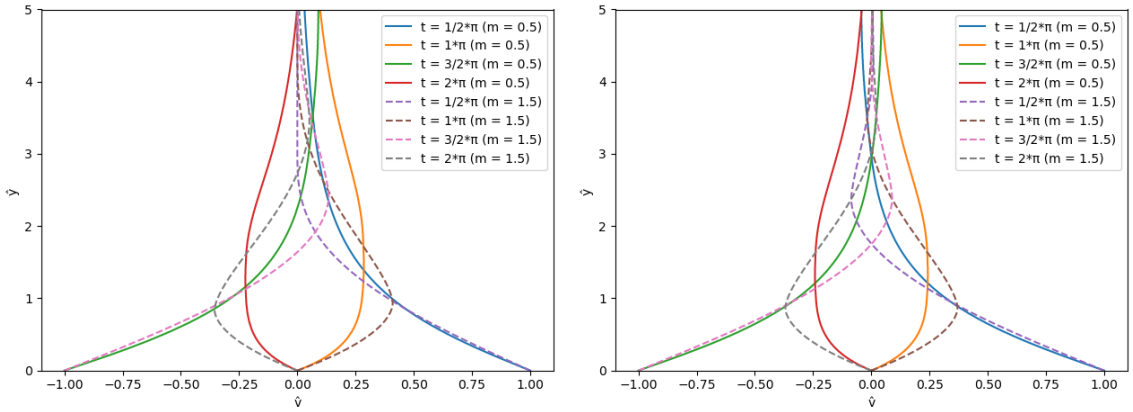

(a) Developing flow (b) Fully developed flow

Figure 4.5: Dimensionless velocity profile plots for different flow index m at constant κ. Using $\kappa = 0.83$ with the used rheological properties sets: $m_1 = 0.5$, $K_{m_1} = 2.5 \cdot 10^3$ [Pa·s^m] and $m_2 = 1.5$, $K_{m_2} = 2.79 \cdot 10^{-10}$ [Pa·s^m].

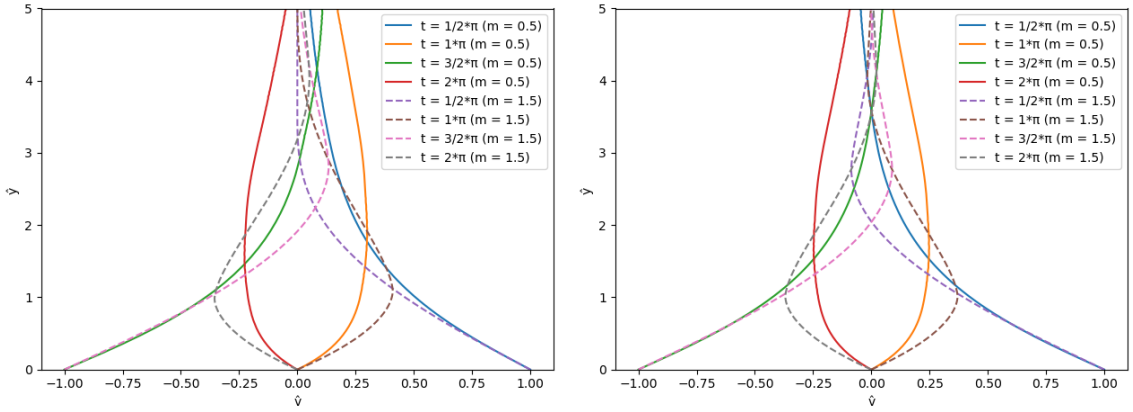

(a) Developing flow (b) Fully developed flow

Figure 4.6: Dimensionless velocity profile plots for different flow index m at constant κ. Using $\kappa = 1.23$ with the used rheological properties sets: $m_1 = 0.5$, $K_{m_1} = 3.68 \cdot 10^2$ [Pa·s^m] and $m_2 = 1.5$, $K_{m_2} = 4.1 \cdot 10^{-10}$ [Pa·s^m].

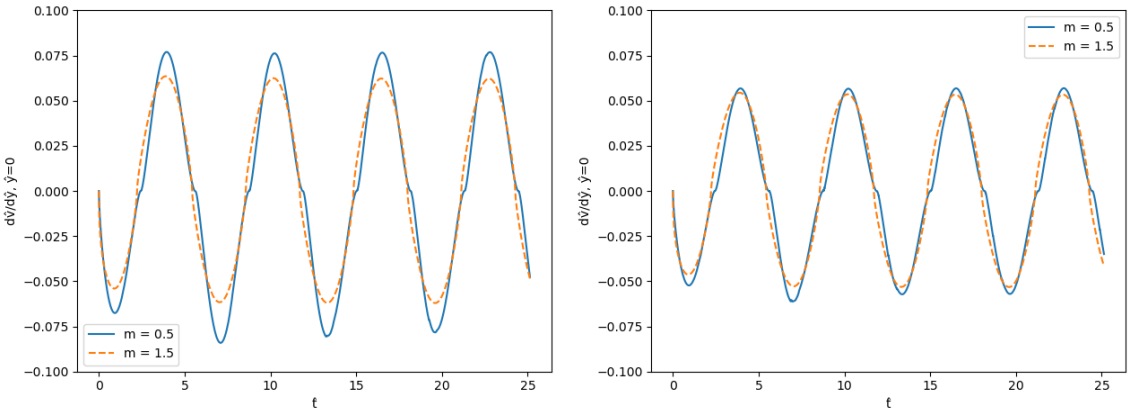

(a) $\kappa = 0.83$ (b) $\kappa = 1.23$

Figure 4.7: *Dimensionless* shear-rate on the boundary plots as function of dimensionless time for different flow index m at constant κ.

The dimensionless shear-rate on the boundary as a function of dimensionless time $\hat{t}$ of figures 4.5 and 4.6 can be determined numerically using equation 3.18. The result for using constant $\kappa = 0.83$ and $\kappa = 1.23$ for the dimensionless shear-rate are shown in the figures 4.7a and 4.7b. The two sets of rheological properties (m, K_m) used to calculated the constant κ are given in the captions of the figures 4.5 and 4.6. The results are shown for four periods to account for the development of the flow. In the calculation of the dimensionless shear-rates of figures 4.7a 4.7b the dimensionless time step $\Delta\hat{t}$ that was used is twice as small as the previously used $\Delta\hat{t} = 2.094 \cdot 10^{-4}$. The reason for this is that fluctuations can occur in the dimensionless shear-rate if its value is around zero and if $m = 0.5$ and K_m is large. Reducing the dimensionless time step reduce these fluctuations.

In figures 4.7a and 4.7b the overlap of the dimensionless shear-rates on the boundary for different flow indices m for equal κ is significant, especially in case of $\kappa = 1.23$. The dimensionless shear-rates show deviant behaviour during the first full period $\hat{t}$ =[0-2π], a result from the development of the flow and after this first period it shows developed behaviour. Also, notice the difference in the shape of the shear-rate around zero for $m = 0.5$ and $m = 1.5$ what seems to arise from the difference between shear-thinning and shear-thickening properties.

4.2.3 Dimensional shear-rates constant κ

The dimensional shear-rate on the boundary as a function of dimensional time for $\kappa = 0.83$ with the rheological properties ($m = 0.5$, $K_m = 2.5 \cdot 10^3$ [Pa·s^m]) and $\kappa = 1.23$ with the rheological properties ($m = 1.5$, $K_m = 4.1 \cdot 10^{-10}$ [Pa·s^m]) are shown in the figures 4.8a and 4.8b. The step sizes used are: $\Delta t = 4.504 \cdot 10^{-12}$ [s], $\Delta y = 6.222 \cdot 10^{-9}$ [m]. The dimensional shear-rates show the same behaviour and overlap as their corresponding dimensionless results from figures 4.7a and 4.7b. This result supports the idea that the constant-κ condition can be used to find equal shear-rates on the boundary for different flow indices, equation 2.47. Therefore, the proposed shear-rate on the boundary of equation 2.48 will be used to solve the Power-law energy equation 2.10.

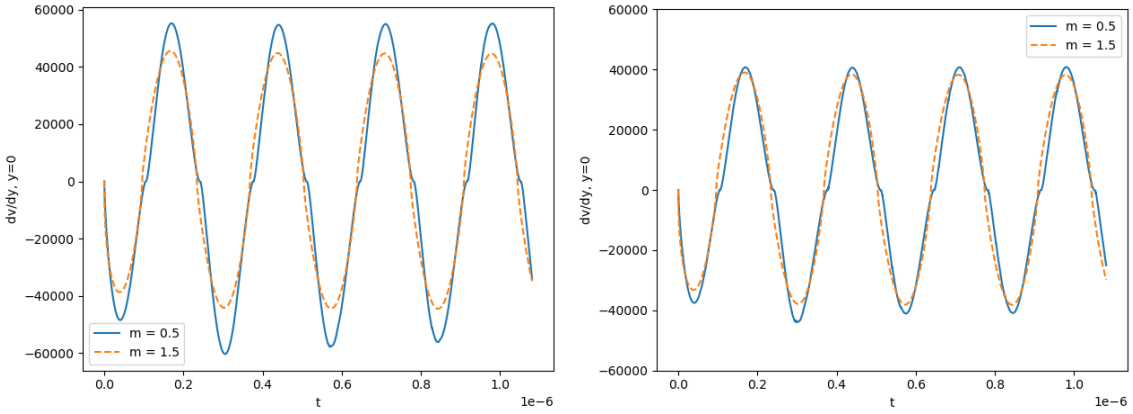

(a) $\kappa = 0.83$ (b) $\kappa = 1.23$

Figure 4.8: *Dimensional* shear-rate on the boundary plots as function of dimensional time for different flow index m at constant κ.

4.3 Methods for retrieving rheological properties

This section shows and discusses the results obtained using methods I, II, III, IV, V and VI described in chapter 3. The Power-Law fluids used in these methods are ketchup, soybean oil and ethylene-glycol. The objective is to retrieve the rheological properties, the flow index m and the consistency index K_m, of these fluids and compare them to their corresponding literature values.

4.3.1 Method I

The results of the retrieved rheological properties using method I of section 3.2.1 for ketchup, soybean oil and ethylene-glycol are displayed in tables 4.1, 4.3 and 4.2 compared to their corresponding literature values. The found flow indices m are very close to the literature values for all fluids but the error in the found consistency index K_m of ketchup and soybean oil is more than $\mathcal{O}(10^1)$ and for ethylene-glycol even more than $\mathcal{O}(10^3)$. It is noted that by changing the fixed frequency between the values of 3.3-4.3 [MHz] the values of K_m change less than 1% between frequencies.
Furthermore, K_m appears to be very sensitive to changes in the found m. This sensitivity in K_m due to a changing m corresponds with results of previous research investigating this method and ideas are proposed to study this phenomenon [14].

Ketchup	Lit. value	**I**
m [-]	0.3	**0.2979**
K_m [Pa· s^m]	6.47	**70.88**

Table 4.1: Literature values of Ketchup for the flow index and consistency index compared to the retrieved values using method I. Used frequency: $\omega = 2\pi \cdot 3.7$ [MHz]. Used step size: $\Delta z = 158.5$ [m].

Soybean oil	Lit. value	**I**
m [-]	0.51	**0.5093**
K_m [Pa· s^m]	2.18	**33.32**

Table 4.2: Literature values of Soybean oil for the flow index and consistency index compared to the retrieved values using method I. Used frequency: $\omega = 2\pi \cdot 3.7$ [MHz]. Used step size: $\Delta z = 2.507$ [m]

Ethylene-Glycol	Lit. value	**I**
m [-]	1.29	**1.289**
K_m [Pa· s^m]	0.0011	**9.271**$\cdot 10^{-7}$

Table 4.3: Literature values of ethylene-glycol for the flow index and consistency index compared to the retrieved values using method I. Used frequency: $\omega = 2\pi \cdot 3.7$ [MHz]. Used step size: $\Delta z = 3.433 \cdot 10^{-5}$ [m]

4.3.2 Method II

The results of the retrieved rheological properties using method II of section 3.2.2 for ketchup, soybean oil and ethylene-glycol are displayed in tables 4.4, 4.5 and 4.6 compared to their corresponding literature values and to the result of method I. Since the total attenuation length of the shear-wave in the waveguide differs significantly per fluid, the immersion depths that will be use are different. However, by taking $l = n_l \cdot \Delta z$ where l is the immersion depth, n_l is the number of steps taken and Δz is the step size per fluid, an immersion depth can be selected which will be at the same position for all fluids relatively.

For all fluids it is noticed that by selecting different immersion depths l the result for the flow index m is unchanged and for the consistency index K_m the change is not more than 2% from the obtained values. The results for the flow index m for all fluids are identical to the results obtained by method I. However, the result for the consistency index K_m worsened for ketchup and soybean oil if using method II compared to method I.

In method I and II to obtain the values for the flow index m the error between the fitted value and the signal, equations 3.25 and 3.29, needs to be minimised, which results in two minimums instead of one, see previous research [14]. This can lead to a faulty prediction of the flow index m. Therefore, the used ranges for m are selected such that only one minimum is obtained.

Ketchup	Lit. value	I	**II**
m [-]	0.3	0.2979	**0.2979**
K_m [Pa· s^m]	6.47	70.88	**111.0**

Table 4.4: Literature values of ketchup for the flow index and consistency index compared to the retrieved values using method I and II. Immersion depth: $l = n_l \cdot \Delta z$ with $n_l = 50$ and $\Delta z = 158.5$ [m].

Soybean oil	Lit. value	I	**II**
m [-]	0.51	0.5093	**0.5093**
K_m [Pa· s^m]	2.18	33.32	**44.37**

Table 4.5: Literature values of soybean oil for the flow index and consistency index compared to the retrieved values using method I and II. Immersion depth: $l = n_l \cdot \Delta z$ with $n_l = 50$ and $\Delta z = 2.507$ [m].

Ethylene-Glycol	Lit. value	I	**II**
m [-]	1.29	1.289	**1.289**
K_m [Pa· s^m]	0.0011	$9.271 \cdot 10^{-7}$	$\mathbf{8.217} \cdot 10^{-7}$

Table 4.6: Literature values of ethylene-glycol for the flow index and consistency index compared to the retrieved values using method I and II. Immersion depth: $l = n_l \cdot \Delta z$ with $n_l = 50$ and $\Delta z = 3.433 \cdot 10^{-5}$ [m].

Added to this issue is the fact that the initial amplitude velocity $B_0(\omega)$, the energy transfer from the transducer to the waveguide, is known numerically but *not* experimentally. Therefore, to get rid of this problem the methods III and IV are proposed, see sections 3.2.3 and 3.2.4. These methods focus on the elimination of $B_0(\omega)$ and retrieving the rheological properties separately.

4.3.3 Method III

The results of the retrieved rheological properties m and K_m using method III of section 3.2.3 for ketchup, soybean oil and ethylene-glycol are displayed in tables 4.7, 4.8 and 4.9 compared to their corresponding literature values and to the results of method I and II. The immersion depths and frequencies which are used per fluid are shown in the captions of the tables.

Selecting different frequencies (ω_1, ω_2) between 3.3-4.3 [MHz] results in a 1.5% deviation of the retrieved consistency indices K_m of tables 4.7, 4.8 and 4.9. The deviation in the flow index m due to different frequency combinations is negligible for ketchup and soybean oil, but a deviation of about 2% is noted in case of ethylene-glycol. It is noted that by using different combinations of immersion depths l in the calculation of m its value changes not more than 1% from the tabulated m for ketchup and soybean oil. The calculated value for the consistency K_m appears to be very sensitive to changes in the calculated m. Also, the results for calculated K_m improve if immersion depths $l < 100 \cdot \Delta z$ are chosen for all fluids.

Ketchup	Lit. value	I	II	**III**
m [-]	0.3	0.2979	0.2979	**0.3498**
K_m [Pa· s^m]	6.47	70.88	111.0	**6.842**

Table 4.7: Literature values of ketchup for the flow index and consistency index compared to the retrieved values using method I, II and III. Immersion depths $l_{1,2} = n_{l_{1,2}} \cdot \Delta z$ used: $l_1 : n_{l_1} = 100$ and $l_2 : n_{l_2} = 200$ with $\Delta z = 158.5$ [m]. Frequencies used: $\omega_1 = 2\pi \cdot 3.6$ [MHz], $\omega_2 = 2\pi \cdot 3.7$ [MHz].

Soybean oil	Lit. value	I	II	**III**
m [-]	0.51	0.5093	0.5093	**0.5636**
K_m [Pa· s^m]	2.18	33.32	44.37	**2.062**

Table 4.8: Literature values of soybean oil for the flow index and consistency index compared to the retrieved values using method I, II and III. Immersion depths $l_{1,2} = n_{l_{1,2}} \cdot \Delta z$ used: $l_1 : n_{l_1} = 100$ and $l_2 : n_{l_2} = 200$ with $\Delta z = 2.507$ [m]. Frequencies used: $\omega_1 = 2\pi \cdot 3.6$ [MHz], $\omega_2 = 2\pi \cdot 3.7$ [MHz].

Ethylene-Glycol	Lit. value	I	II	**III**
m [-]	1.29	1.289	1.289	**1.149**
K_m [Pa· s^m]	0.0011	$9.271{\cdot}10^{-7}$	$8.217{\cdot}10^{-7}$	**0.006456**

Table 4.9: Literature values of ethylene-glycol for the flow index and consistency index compared to the retrieved values using method I, II and III. Immersion depths $l_{1,2} = n_{l_{1,2}} \cdot \Delta z$ used: $l_1 : n_{l_1} = 100$ and $l_2 : n_{l_2} = 200$ with $\Delta z = 3.433 \cdot 10^{-5}$ [m]. Frequencies used: $\omega_1 = 2\pi \cdot 3.6$ [MHz], $\omega_2 = 2\pi \cdot 3.7$ [MHz].

The calculated values of the flow index m of method III in tables 4.7, 4.8 and 4.9 deviate significantly from their literature values and the results of method I and II. The found values for the consistency index K_m using method III are of the same order of magnitude as their literature values. However, the equation used to calculated K_m for ketchup, soybean oil and ethylene-glycol in method III, equation 3.38, uses value for m from tables 4.7, 4.8 and 4.9. Since these values for m are not equal to their literature values it is believed that the found results of K_m having the same order of magnitude as the literature values for ketchup, soybean oil and ethylene-glycol are not accurate.

4.3.4 Method IV

The results of the retrieved rheological properties m and K_m using method IV of section 3.2.4 for ketchup, soybean oil and ethylene-glycol are displayed in tables 4.10, 4.11 and 4.12 compared to their corresponding literature values and to the results of method I, II, III. The immersion depths and frequencies which are used per fluid are shown in the captions of the tables.

Ketchup	Lit. value	I	II	III	**IV**
m [-]	0.3	0.2979	0.2979	0.3498	**0.2997**
K_m [Pa· s^m]	6.47	70.88	111.0	6.842	**9.854**$\cdot 10^{-5}$

Table 4.10: Literature values of ketchup for the flow index and consistency index compared to the retrieved values using method I, II, III and IV. Immersion depths $l_{1,2} = n_{l_{1,2}} \cdot \Delta z$ used: $l_1 : n_{l_1} = 100$ and $l_2 : n_{l_2} = 200$ with $\Delta z = 158.5$ [m]. Frequencies used: $\omega_1 = 2\pi \cdot 3.6$ [MHz], $\omega_2 = 2\pi \cdot 3.7$ [MHz].

Soybean oil	Lit. value	I	II	III	**IV**
m [-]	0.51	0.5093	0.5093	0.5636	**0.5096**
K_m [Pa· s^m]	2.18	33.32	44.37	2.062	**9.286**$\cdot 10^{-5}$

Table 4.11: Literature values of soybean oil for the flow index and consistency index compared to the retrieved values using method I, II, III and IV. Immersion depths $l_{1,2} = n_{l_{1,2}} \cdot \Delta z$ used: $l_1 : n_{l_1} = 100$ and $l_2 : n_{l_2} = 200$ with $\Delta z = 2.507$ [m]. Frequencies used: $\omega_1 = 2\pi \cdot 3.6$ [MHz], $\omega_2 = 2\pi \cdot 3.7$ [MHz].

Ethylene-Glycol	Lit. value	I	II	III	**IV**
m [-]	1.29	1.289	1.289	1.149	**1.292**
K_m [Pa· s^m]	0.0011	$9.271 \cdot 10^{-7}$	$8.217 \cdot 10^{-7}$	0.006456	**0.2529**

Table 4.12: Literature values of ethylene-glycol for the flow index and consistency index compared to the retrieved values using method I, II, III and IV. Immersion depths $l_{1,2} = n_{l_{1,2}} \cdot \Delta z$ used: $l_1 : n_{l_1} = 100$ and $l_2 : n_{l_2} = 200$ with $\Delta z = 3.433 \cdot 10^{-5}$ [m]. Frequencies used: $\omega_1 = 2\pi \cdot 3.6$ [MHz], $\omega_2 = 2\pi \cdot 3.7$ [MHz].

The retrieved results using method IV for the flow index m for ketchup, soybean oil and ethylene-glycol are close to their corresponding literature values, but the results for the consistency index K_m deviate still significantly from the literature values. The change to m if selecting other frequencies within the range 3.3-4.3 [MHz] in equation 3.46 is negligible all fluid. Selecting different frequency combinations between 3.3-4.3 [MHz] in equation 3.47 results in a 1.5% deviation from the retrieved consistency indices K_m for all fluids. Different selections of immersion depths have a negligible effect on the value m in equation 3.46 and only about 1% change in determining the value of K_m in equation 3.47.

The results of method IV show that flow index m can be determined accurately using equation 3.46 without needing an exact expression for the shear-rate on the boundary since most of its terms are divided out. The only terms necessary for the calculation are the measured velocity amplitudes at two known frequencies and two known immersion depths.

The proposed shear-rate I

The proposed shear-rate on the boundary of equation 2.37 in section 2.6.2 is used in the methods I, II, III and IV in order to retrieve the rheological properties of Power-law fluids. This equation is based on the assumption that shear-rates on boundary in a Power-law fluid

are independent of the flow index m, resulting in $K_m = K_1 = \mu_0$. However, by taking a closer look at the units of K_m [Pa·s^m] and μ_0 [Pa·s] it can see that they are not the same. Therefore, the condition of $K_m = K_1 = \mu_0$ is thought to be incorrect. This results in the conclusion that the shear-rate on the boundary proposed in equation 2.37 is wrong.

4.3.5 Method V

The results of the retrieved rheological properties m and K_m using method V of section 3.2.5 for ketchup, soybean oil and ethylene-glycol are displayed in tables 4.13, 4.14 and 4.15 compared to their corresponding literature values and to the results of method I, II, III and IV. The immersion depths and frequencies which are used per fluid are shown in the captions of the tables.

The calculated values of the flow index m for ketchup, soybean oil and ethylene-glycol are close to their corresponding literature values. These calculated flow indices are also equal to the flow indices calculated with method IV. This was expected since the equations to calculated the flow index in both methods are equal, equation 3.46 and equation 3.54 respectively. The results of the calculated consistency indices in tables 4.13, 4.14 and 4.15 deviate from the literature values, but appear to have improved compared to method IV.

Method V uses the numerically known value of the initial velocity amplitude B_0 in order to determine K_m. However, as mentioned section 3.2.3 the value of this term is unknown experimentally. This was reason that methods III and IV were developed in the first place. Therefore, if $B_0(\omega)$ cannot be determined experimentally method V seems to be unsuitable for experimental use.

Ketchup	Lit. value	I	II	III	IV	**V**
m [-]	0.3	0.2979	0.2979	0.3498	0.2997	**0.2997**
K_m [Pa· s^m]	6.47	70.88	111.0	6.842	$9.854{\cdot}10^{-5}$	**0.2868**

Table 4.13: Literature values of ketchup for the flow index and consistency index compared to the retrieved values using method I, II, III, IV and V. Immersion depths $l_{1,2} = n_{l_{1,2}} \cdot \Delta z$ used: $l_1 : n_{l_1} = 100$ and $l_2 : n_{l_2} = 200$ with $\Delta z = 158.5$ [m]. Frequencies used: $\omega_1 = 2\pi \cdot 3.6$ [MHz], $\omega_2 = 2\pi \cdot 3.7$ [MHz].

Soybean oil	Lit. value	I	II	III	IV	**V**
m [-]	0.51	0.5093	0.5093	0.5636	0.5096	**0.5096**
K_m [Pa· s^m]	2.18	33.32	44.37	2.062	$9.286{\cdot}10^{-5}$	**1.056**

Table 4.14: Literature values of soybean oil for the flow index and consistency index compared to the retrieved values using method I, II, III, IV and V. Immersion depths $l_{1,2} = n_{l_{1,2}} \cdot \Delta z$ used: $l_1 : n_{l_1} = 100$ and $l_2 : n_{l_2} = 200$ with $\Delta z = 2.507$ [m]. Frequencies used: $\omega_1 = 2\pi \cdot 3.6$ [MHz], $\omega_2 = 2\pi \cdot 3.7$ [MHz].

Ethylene-Glycol	Lit. value	I	II	III	IV	**V**
m [-]	1.29	1.289	1.289	1.149	1.292	**1.292**
K_m [Pa· s^m]	0.0011	$9.271{\cdot}10^{-7}$	$8.217{\cdot}10^{-7}$	0.006456	0.2529	**0.07048**

Table 4.15: Literature values of ethylene-glycol for the flow index and consistency index compared to the retrieved values using method I, II, III, IV and V. Immersion depths $l_{1,2} = n_{l_{1,2}} \cdot \Delta z$ used: $l_1 : n_{l_1} = 100$ and $l_2 : n_{l_2} = 200$ with $\Delta z = 3.433 \cdot 10^{-5}$ [m]. Frequencies used: $\omega_1 = 2\pi \cdot 3.6$ [MHz], $\omega_2 = 2\pi \cdot 3.7$ [MHz].

4.3.6 Method VI

In this section, the results of the retrieved rheological properties m and K_m using method VI of section 3.2.6 for ketchup, soybean oil and ethylene-glycol are shown. Method VI uses two different approaches to calculate the value of the consistency index, namely Approach A (numerical) and Approach B (experimental).

Approach A

Tables 4.16, 4.17 and 4.18 show the obtained results using Approach A of m and K_m, calculated with equations 3.62 and 3.63. The used averaged apparent viscosities for each fluid per frequency $\langle \mu_{app}(\omega) \rangle$ are calculated by averaging the result of equation 3.64 over time and their value is given in the captions of the corresponding tables. The apparent viscosities as a function of time per fluid for frequency $\omega = 2\pi \cdot 3.7$ [MHz] using equation 3.64 are shown in figure 4.9. The immersion depths and frequencies which are used per fluid are also shown in the captions of the tables.

The results of the retrieved consistency index K_m using Approach A of method VI have improved for all fluids compared to previous results shown in tables 4.13, 4.14 and 4.15. This gives reason to believe that by changing the constant viscosity of a Newtonian fluid to a time-averaged numerical apparent viscosity of a Power-law fluid (equation 2.52), the shear-rate of a Power-law fluid on the boundary can be estimated reasonably.

Ketchup	Lit. value	**VI (A)**
m [-]	0.3	**0.2997**
K_m [Pa· s^m]	6.47	**6.914**

Table 4.16: Literature values of the rheological properties of ketchup compared to the values retrieved using Method VI and Approach A. Immersion depths $l_{1,2} = n_{l_{1,2}} \cdot \Delta z$ used: $l_1 : n_{l_1} = 100$ and $l_2 : n_{l_2} = 200$ with $\Delta z = 158.5$ [m]. Frequencies used: $\omega_1 = 2\pi \cdot 3.6$ [MHz], $\omega_2 = 2\pi \cdot 3.7$ [MHz] Time-averaged apparent viscosity's used: $\langle \mu_{app}(\omega_1) \rangle = 1.434 \cdot 10^{-3}$ [Pa·s] and $\langle \mu_{app}(\omega_2) \rangle = 1.417 \cdot 10^{-3}$ [Pa·s].

Soybean oil	Lit. value	**VI (A)**
m [-]	0.51	**0.5095**
K_m [Pa· s^m]	2.18	**2.861**

Table 4.17: Literature values of the rheological properties of soybean oil compared to the values retrieved using Method VI and Approach A. Immersion depths $l_{1,2} = n_{l_{1,2}} \cdot \Delta z$ used: $l_1 : n_{l_1} = 100$ and $l_2 : n_{l_2} = 200$ with $\Delta z = 2.507$ [m]. Frequencies used: $\omega_1 = 2\pi \cdot 3.6$ [MHz], $\omega_2 = 2\pi \cdot 3.7$ [MHz]. Time-averaged apparent viscosity's used: $\langle \mu_{app}(\omega_1) \rangle = 7.317 \cdot 10^{-3}$ [Pa·s] and $\langle \mu_{app}(\omega_2) \rangle = 7.242 \cdot 10^{-3}$ [Pa·s].

Ethylene-Glycol	Lit. value	**VI (A)**
m [-]	1.29	**1.292**
K_m [Pa· s^m]	0.0011	**5.002**$\cdot 10^{-4}$

Table 4.18: Literature values of the rheological properties of ethylene-glycol compared to the values retrieved using Method VI and Approach A. Immersion depths $l_{1,2} = n_{l_{1,2}} \cdot \Delta z$ used: $l_1 : n_{l_1} = 100$ and $l_2 : n_{l_2} = 200$ with $\Delta z = 3.433 \cdot 10^{-5}$ [m]. Frequencies used: $\omega_1 = 2\pi \cdot 3.6$ [MHz], $\omega_2 = 2\pi \cdot 3.7$ [MHz]. Time-averaged apparent viscosity's used: $\langle \mu_{app}(\omega_1) \rangle = 3.080 \cdot 10^{-2}$ [Pa·s] and $\langle \mu_{app}(\omega_2) \rangle = 3.106 \cdot 10^{-2}$ [Pa·s].

Approach B

The results using Approach B to calculated m and K_m, using equations 3.62 and 3.66 respectively, are shown in tables 4.19, 4.20 and 4.21 compared to their corresponding literature values and to the results of method VI (A). The immersion depths and frequencies which are used per fluid are shown in the captions of the tables. In the figures 4.10, 4.11 and 4.12 the apparent viscosity and rheology calculated with the retrieved values of the rheological properties are shown for each fluid.

The results found for the flow indices are unchanged compared to the result of method IV (A) for all fluids since the same equation to calculate m is used, equation 3.62. The retrieved values for the consistency indices have in all cases the same order of magnitude as their literature values. Knowing that the proposed analytical time-averaged apparent viscosity of equation 3.65 is not entirely correct by assuming $\dot{\gamma}_{PL} \sim \omega$, it results in similar values as produced by method VI (A). However, the results using method VI (B) can be obtained experimentally, unlike the results of method VI (A) which need a numerical solution to the apparent viscosity.
The result of experimental apparent viscosity plots of ketchup and soybean oil of figures 4.10, 4.11 seem to be a reasonable estimate of the literature plot when the shear-rate is larger than 100 [s^{-1}]. The experimental apparent viscosity plot of ethylene-glycol, figure 4.12, seems to be a reasonable estimate of the literature plot when the shear-rate is smaller than 100 [s^{-1}].

The next step is to investigate what needs to be changed to the expression of the shear-rate on the boundary of a Power-law fluid 2.52 such that by using the numerical apparent viscosity, the results of the retrieved consistency indices correspond to their literature values.

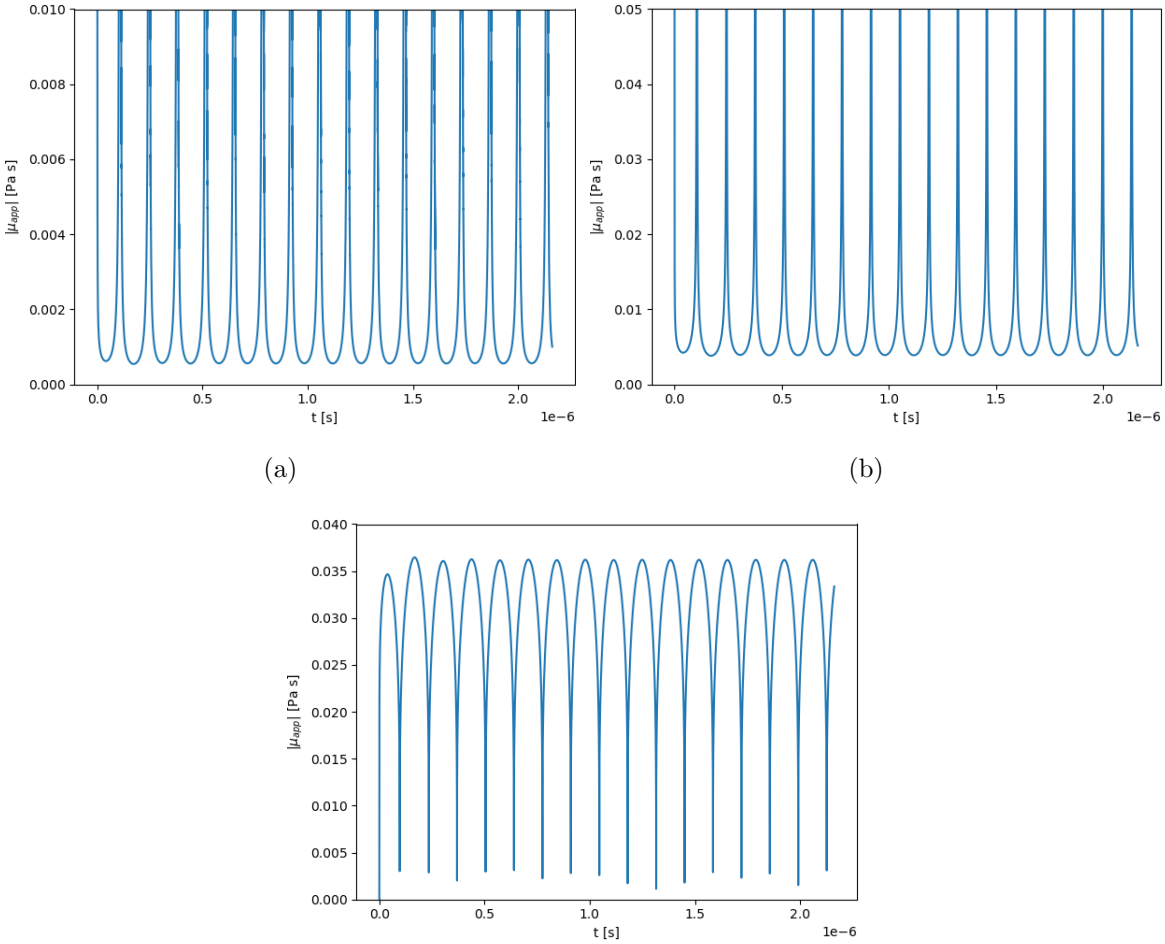

Figure 4.9: Absolute apparent viscosity at the boundary as function of time for the fluids ketchup (a), soybean oil (b) and ethylene-glycol (c) at a frequency $\omega = 2\pi \cdot 3.7$ [MHz]. The results are created using the corresponding velocity profiles of the fluids, see figures 4.1a, 4.2a and 4.3a.

Ketchup	Lit. value	VI (A)	**VI (B)**
m [-]	0.3	0.2997	**0.2997**
K_m [Pa· s^m]	6.47	6.914	**3.874**

Table 4.19: Literature values of the rheological properties of ketchup compared to the values retrieved by using Method VI (A) and Method (B). Immersion depths $l_{1,2} = n_{l_{1,2}} \cdot \Delta z$ used: $l_1 : n_{l_1} = 100$ and $l_2 : n_{l_2} = 200$ with $\Delta z = 158.5$ [m]. Frequencies used: $\omega_1 = 2\pi \cdot 3.6$ [MHz], $\omega_2 = 2\pi \cdot 3.7$ [MHz].

Soybean oil	Lit. value	VI (A)	**VI (B)**
m [-]	0.51	0.5095	**0.5095**
K_m [Pa· s^m]	2.18	2.861	**1.150**

Table 4.20: Literature values of the rheological properties of soybean oil compared to the values retrieved by using Method VI (A) and Method (B). Immersion depths $l_{1,2} = n_{l_{1,2}} \cdot \Delta z$ used: $l_1 : n_{l_1} = 100$ and $l_2 : n_{l_2} = 200$ with $\Delta z = 2.507$ [m]. Frequencies used: $\omega_1 = 2\pi \cdot 3.6$ [MHz], $\omega_2 = 2\pi \cdot 3.7$ [MHz].

Ethylene-Glycol	Lit. value	VI (A)	**VI (B)**
m [-]	1.29	1.292	**1.292**
K_m [Pa· s^m]	0.0011	$5.002 \cdot 10^{-4}$	**0.001302**

Table 4.21: Literature values of the rheological properties of ethylene-glycol compared to the values retrieved by using Method VI (A) and Method (B). Immersion depths $l_{1,2} = n_{l_{1,2}} \cdot \Delta z$ used: $l_1 : n_{l_1} = 100$ and $l_2 : n_{l_2} = 200$ with $\Delta z = 3.433 \cdot 10^{-5}$ [m]. Frequencies used: $\omega_1 = 2\pi \cdot 3.6$ [MHz], $\omega_2 = 2\pi \cdot 3.7$ [MHz].

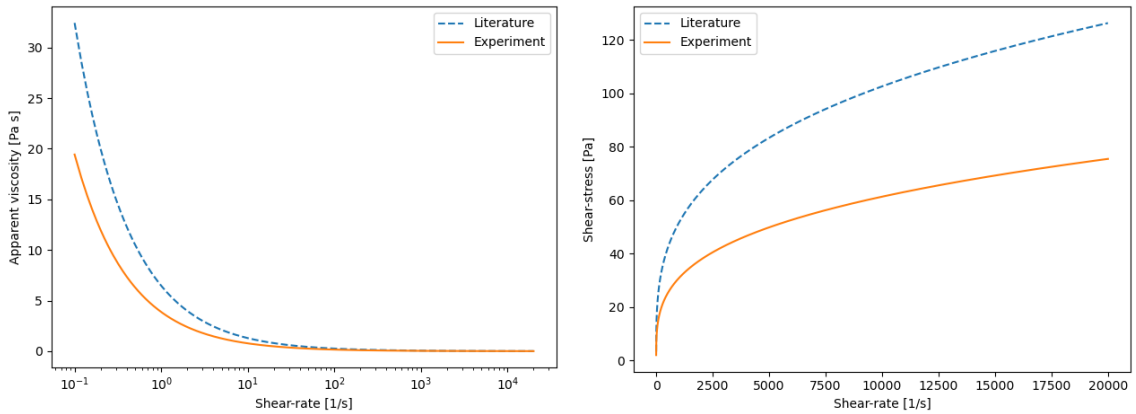

(a) Apparent viscosity

(b) Rheology

Figure 4.10: **Ketchup** (Lit: $m = 0.3$, $K_m = 6.47$), (Experiment = Method VI (B): $m = 0.2997$, $K_m = 3.874$); Apparent viscosity (a) and rheology (b) plot using literature and experimental rheological properties. The step sizes used are: $\Delta t = 9.009 \cdot 10^{-12}$ [s], $\Delta y = 4.677 \cdot 10^{-9}$ [m], $\Delta z = 158.5$ [m] and used frequency: $f = 3.7$ [MHz].

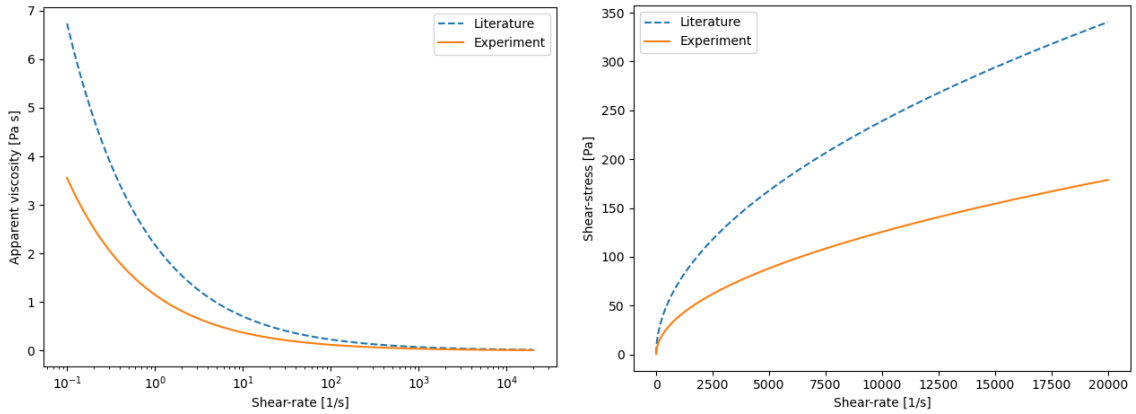

(a) Apparent viscosity (b) Rheology

Figure 4.11: **Soybean oil** (Lit: $m = 0.51$, $K_m = 2.18$), (Experiment = Method VI (B): $m = 0.5095$, $K_m = 1.150$); Apparent viscosity (a) and rheology (b) plot using literature and experimental rheological properties. The step sizes used are: $\Delta t = 9.009 \cdot 10^{-12}$ [s], $\Delta y = 2.226 \cdot 10^{-8}$ [m], $\Delta z = 2.507$ [m] and used frequency: $f = 3.7$ [MHz].

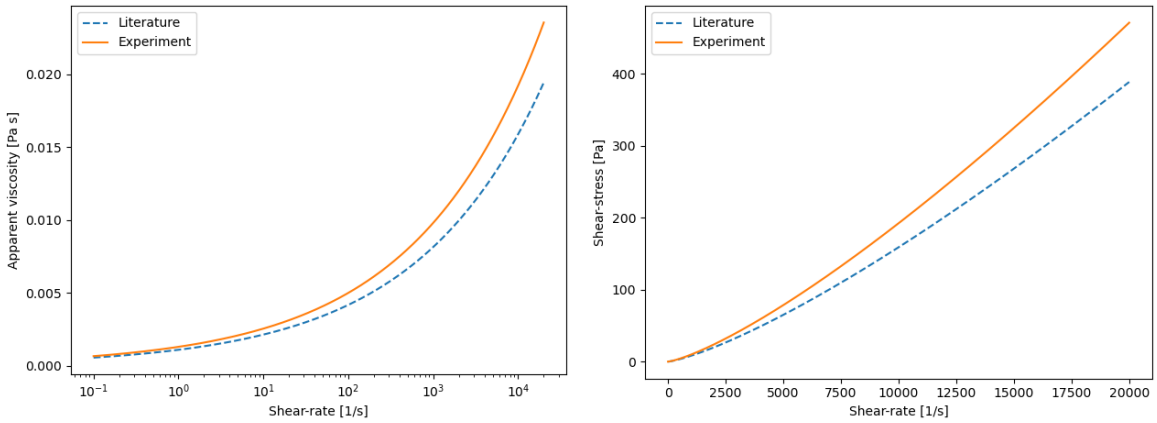

(a) Apparent viscosity (b) Rheology

Figure 4.12: **Ethylene-Glycol** ($m = 1.3$, $K_m = 0.0011$), (Experiment = Method VI (B): $m = 1.292$, $K_m = 0.001302$); Apparent viscosity (a) and rheology (b) plot using literature and experimental rheological properties. The step sizes used are: $\Delta t = 9.009 \cdot 10^{-12}$ [s], $\Delta y = 6.831 \cdot 10^{-8}$ [m], $\Delta z = 3.433 \cdot 10^{-5}$ [m] and used frequency: $f = 3.7$ [MHz].

Chapter 5

Conclusion and recommendation

The goal of this research was to develop methods of determining the rheological properties of Power-law fluids from amplitude measurements of the ultrasonic shear-wave waveguide viscometer using a numerical model. To achieve this goal an analytical expression of the shear-rate in a Power-law fluid is necessary. In this research three analytical expression of the shear-rate in a Power-law fluid are used. The fluids used in this research are ketchup (shear-thinning), soybean oil (shear-thinning) and ethylene-glycol (shear-thickening).
The methods I, II, III and IV are used to find the rheological properties m and K_m with an expression of the shear-rate based on the result of Ai & Vafai [13], first proposed by Rohde [11]. Methods I and II gave accurate results for the flow index m, but the results for the consistency index K_m deviated significantly from the literature values for all fluids. These methods also make use of the experimentally unknown initial velocity amplitude which makes them unsuitable during physical measurements. Method III gave inaccurate results for the flow index m for all fluids, but the results for the consistency index K_m are in the same order of magnitude as their literature values. However, the results for K_m are deemed incorrect. Method IV gave accurate results for the flow index m but inaccurate result for the consistency index K_m. Although, the shear-rate used in methods I, II, III, IV turned out to be incorrect, the expression used to determine the flow index m remains valid and experimentally usable. Method V uses a different expression of the shear-rate in a Power-law fluid compared to methods I, II, III and IV. The results of this method for the flow index m are unchanged compared to results of method IV and the values for the consistency indices K_m improved compared to method IV but still deviated from the literature values.
Method VI uses an alternative expression of the shear-rate in a Power-law fluid compared to methods I, II, III, IV and V. Within method VI two approaches are used to determine the rheological properties m, K_m, namely: Approach A and Approach B. Approach A can only be used numerically, but Approach B can be used experimentally. Both Approach A and Approach B of method VI gave accurate results for the flow index m and the results of the consistency indices K_m have the same order of magnitude as their literature values.
In future studies the shear-rate on the boundary of Power-law fluids needs to be studied more extensively to obtain more accurate results for the consistency indices. Also, the numerical viscometer needs to be extended for other types of fluids such as Bingham and Casson fluids. This will eventually contribute to the final goal of SAMOSAFER to ensure that the MSFR can comply with all expected regulations in 30 years' time.

Bibliography

[1] World-nuclear.org. (2021). Generation IV Nuclear Reactors: WNA - World Nuclear Association. [online] Available at: http://www.world-nuclear.org/information-library/nuclear-fuel-cycle/nuclear-power-reactors/generation-iv-nuclear-reactors.aspx [Accessed 3 June 2021].

[2] European Commission (2012). *Energy Roadmap 2050* Luxembourg: Office for Official Publications of the European Communities.

[3] SAMOSAFER. (2021). Project – SAMOSAFER. [online] Available at: http://samosafer.eu/project/ [Accessed 31 may. 2021].

[4] Jérôme Serp, Michel Allibert, Ondřej Beneš, Sylvie Delpech, Olga Feynberg, Véronique Ghetta, Daniel Heuer, David Holcomb, Victor Ignatiev, Jan Leen Kloosterman, et al. The molten salt reactor (msr) in generation iv: overview and perspectives. Progress in Nuclear Energy, 77:308–319, 2014.

[5] E. Capelli, O. Beneš, R.J.M. Konings, Thermodynamic assessment of the LiF–ThF4–PuF3–UF4 system, *Journal of Nuclear Materials*, Volume 462, Pages 43-53, 2015.

[6] Roberto Serrano-López, Jordi Fradera, and Santiago Cuesta-López. Molten salts database for energy applications. *Chemical Engineering and Processing: Process Intensification*, 73:87–102, 2013.

[7] WP Mason, WO Baker, HJ McSkimin, and JH Heiss. Measurement of shear elasticity and viscosity of liquids at ultrasonic frequencies. *Physical Review*, 75(6):936, 1949.

[8] Thomas K Vogt, JS Lowe, and Peter Cawley. Measurement of the material properties of viscous liquids using ultrasonic guided waves. *IEEE transactions on ultrasonics, ferroelectrics, and frequency control*, 51(6):737–747, 2004.

[9] T Stevenson, DG Martin, PI Cowin, A Blumfield, AJ Bell, TP Comyn, and PM Weaver. Piezoelectric materials for high temperature transducers and actuators. *Journal of Materials Science: Materials in Electronics*, 26(12):9256–9267, 2015

[10] Frédéric Bert Cegla. *Ultrasonic waveguide sensors for fluid characterisation and remote sensing*. PhD thesis, Imperial College London, 2006.

[11] M. Rohde, Determining the rheology of power law fluids with a wave guide at high-frequency shear waves, internal report. Technical report, Delft University of Technology, 2020

[12] Remco Rook. Viscosity determination of newtonian fluids using shear ultrasonic guided wave attenuation. Master's thesis, TU Delft, March 2020.

[13] L Ai and K Vafai. An investigation of stokes' second problem for non-newtonian fluids. Numerical Heat Transfer, Part A, 47(10):955–980, 2005.

[14] Lotte Borstlap. Numerical study on the determination of the rheological properties of power-law fluids in the ultrasonic waveguide experiment. Bachelor's thesis, TU Delft, August 2020.

[15] R.F. Mudde H.E.A van den Akker. Fysische transportverschijnselen. VSSD, TU Delft, 2013.

[16] Simscale.com. (2021). Non-Newtonian models. [online] Available at: https://www.simscale.com/docs/simulation-setup/materials/non-newtonian-models/ [Accessed 3 June 2021].

[17] Acheson, David J. Elementary fluid dynamics. Oxford University Press, 1990.

[18] M. Zijlema. *Computational Modelling of Flow and Transport*, Department Hydraulic Engineering, TU Delft, 2015

[19] Isaacson, E. and Keller, H., 1996. Analysis of numerical methods. New York: Dover.

[20] John C. Tannehill; Dale A. Anderson; Richard H. Pletcher (1997). Computational Fluid Mechanics and Heat Transfer (2nd ed.). Taylor & Francis. ISBN 1-56032-046-X.

[21] Léon Peter Bernard Marie Janssen and Marinus Maria Cornelis Gerardus Warmoeskerken. Transport phenomena data companion. Hodder Arnold, 1987.

[22] Vojtěch Kumbár, Sylvie Ondrušíková, and Šárka Nedomová. Rheological properties of tomato ketchup. Potravinarstvo Slovak Journal of Food Sciences, 13(1):730–734, 2019.

[23] Nelson Moraga, Alejandra Torres, Abel Guarda, and María José Galotto. Non-newtonian canned liquid food, unsteady fluid mechanics and heat transfer prediction for pasteurization and sterilization. Journal of Food Process Engineering, 34(6):2000–2025, 2011.

[24] Richard G Green and Richard G Griskey. Rheological behavior of dilatant (shear-thickening) fluids. part i. experimental and data. Transactions of the Society of Rheology, 12(1):13–25, 1968.

[25] Harris, C.R., Millman, K.J., van der Walt, S.J. et al. Array programming with NumPy. Nature 585, 357–362 (2020). DOI: 0.1038/s41586-020-2649-2.